TM-70-2011-1

TECHNICAL MEMORANDUM

AN ANALYTICAL SOLUTION TO PATCHED CONIC TRAJECTORIES SATISFYING INITIAL AND FINAL BOUNDARY CONDITIONS

Bellcomm

BELLCOMM, INC.
955 L'ENFANT PLAZA NORTH, S.W., WASHINGTON, D.C. 20024

COVER SHEET FOR TECHNICAL MEMORANDUM

TITLE-An Analytical Solution to Patched Conic Trajectories Satisfying Initial and Final Boundary Conditions

TM-70-2011-1

DATE-November 30, 1970

FILING CASE NO(S)-310

AUTHOR(S)-K. M. Carlson

FILING SUBJECT(S) (ASSIGNED BY AUTHOR(S))-
Patched-Conic Trajectories
Interplanetary Trajectories
Lunar Trajectories
Trajectory Analysis
Celestial Mechanics

ABSTRACT

Analytical expressions for patched-conic trajectories are derived, thus providing the analyst with a tool for the calculation of spacecraft trajectories between two bodies and for understanding the behavior of these trajectories as the mission constraints are varied. Two sets of equations are developed which allow an analytical solution to spacecraft trajectories between two large central bodies and which satisfy boundary conditions at both bodies. The derivations of these equation sets are based on patched-conic analysis. The independent parameters required are the spacecraft angular momentum and inclination with respect to the more massive body, and the spacecraft angular momentum, energy, and inclination with respect to the less massive body, or equivalent quantities. These equation sets provide a good approximation to the sphere of influence trajectory patch point over essentially the entire range of possible trajectories. Having obtained the patch point, the spacecraft state vector is easily obtained.

BELLCOMM, INC.
955 L'ENFANT PLAZA NORTH, S.W. WASHINGTON, D.C. 20024

SUBJECT: An Analytical Solution to Patched Conic Trajectories Satisfying Initial and Final Boundary Conditions Case 310

DATE: November 30, 1970

FROM: K. M. Carlson

TM-70-2011-1

TECHNICAL MEMORANDUM

1.0 INTRODUCTION

The study of spacecraft trajectories between two bodies does not yield to mathematical analysis as well as trajectories about a single body. Consequently, the understanding of such trajectories has been difficult and, to an extent, intuitive. This memorandum provides a major simplification in the analysis of such trajectories.

The analysis contained here is based on the patched-conic approximation to trajectories between two large central bodies. In Reference 1, the author carried out a detailed analysis of the basic elements of the trajectory patch point locus on the sphere of influence. These elements were identified and described on a geometrical basis. Using the geometrical insights gained in Reference 1, equations are derived in this memorandum which predict the location of the patch point using trajectory parameters from both inside and outside the sphere of influence. Once the patch point is located, the trajectory state vector can be easily calculated, and hence the spacecraft position may be found for any time. The trajectory parameters required by the patch point equations can be thought of as being the elements of the trajectory. There are six such elements, just as there are six elements of a trajectory about a single body. Since the parameters describe features both inside and outside the sphere of influence, obtaining a trajectory with desired characteristics is considerably simplified.

Two equation sets are derived. One set is valid over essentially the entire regime of possible trajectories. The other equation set is valid only for trajectories at the high energy end of the trajectory regime; however, this set is considerably simpler than the set with general validity.

The basic elements of the sphere of influence patch point locus will be discussed first without proof.

The patch point equation sets will then be derived and the necessary proofs supplied. Finally, the validity of the analysis will be illustrated numerically, and some useful techniques and approximations will be presented. The patched-conic equation sets are restated in Appendix B for easy reference.

Several terms which are used frequently in the analysis bear some explanation. The two large central bodies are referred to as the major body and the minor body, the major body being the more massive of the two. The sphere of influence is a spherical region surrounding the minor body within which only the minor body's gravitational field is assumed to operate. All the rest of space is assumed to be influenced only by the major body's gravitational field. Trajectories are named descriptively. Thus, a rectilinear trajectory is one which rises and/or descends vertically with respect to its central body, i.e., the spacecraft position and velocity vectors are colinear. A dual rectilinear trajectory passes between the major and minor bodies and consists of rectilinear trajectory segments centered at each body. A single rectilinear trajectory again passes between the two bodies but has only one body-centered segment which is rectilinear. A non-rectilinear trajectory is one such that neither of its body-centered portions is rectilinear. A restatement of these definitions, as well as a list of symbols used, is contained in Appendix A for easy reference.

2.0 STRUCTURE OF THE SPHERE OF INFLUENCE PATCH POINT LOCUS

The sphere of influence patch point locus for non-rectilinear trajectories can be constructed from the dual and single rectilinear trajectory patch point loci with the same energy. Figure 1 shows the dual and single rectilinear trajectory patch point loci for trajectories with identical minor body referenced energies.

It is seen from Figure 1 that the dual rectilinear patch point locus (C) is a single point lying on the intersection of the sphere of influence and the minor body orbital plane. The major-body-centered and minor-body-centered single-rectilinear trajectory loci (A and B) are closed curves containing the dual rectilinear patch point. Each point of the single rectilinear trajectory loci (e.g., A and B) represents a different trajectory plane orientation. The sizes of the single rectilinear loci are dependent on the angular momenta of the non-rectilinear trajectory segments. Angular momentum is, in turn, related to pericenter radius. Note that the

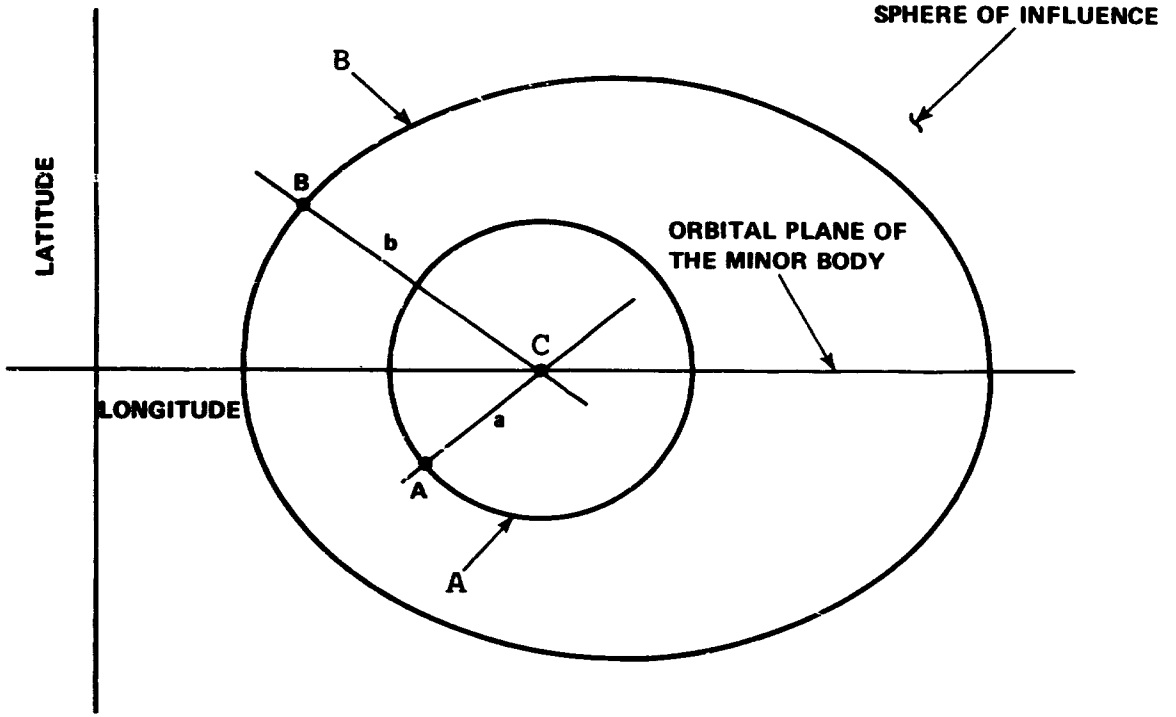

A – MAJOR-BODY-CENTERED SINGLE-RECTILINEAR PATCH POINT LOCUS.

A – PATCH POINT FOR A MAJOR-BODY-CENTERED SINGLE-RECTILINEAR TRAJECTORY WHOSE PLANE FORMS THE TRACE a ON THE SPHERE OF INFLUENCE.

B – MINOR-BODY-CENTERED SINGLE-RECTILINEAR PATCH POINT LOCUS.

B – PATCH POINT FOR A MINOR-BODY-CENTERED SINGLE-RECTILINEAR TRAJECTORY WHOSE PLANE FORMS THE TRACE b ON THE SPHERE OF INFLUENCE.

C – DUAL RECTILINEAR PATCH POINT.

FIGURE 1 – BASIC TYPES OF SPHERE OF INFLUENCE PATCH POINT LOCI

trajectory planes for single rectilinear trajectories pass through the dual rectilinear patch point. That is, the node line between the spacecraft trajectory plane and the minor body orbital plane is the path of a dual rectilinear trajectory with the same minor body referenced energy.

Figure 2 shows the patch point locus for non-rectilinear trajectories. It will be shown that this locus can be constructed as follows:

1. Calculate the dual and single rectilinear trajectory patch point loci (A, B, and C) for the desired trajectory energy and angular momenta as shown in Figure 1.

2. Select the minor-body-centered single-rectilinear patch point (B) representing the major-body-centered trajectory plane desired.

3. Transpose the major-body-centered single-rectilinear patch point locus (A) to A' so that the interior point originally coinciding with the dual rectilinear patch point (C) now coincides with the point B selected in Step 2.

Each point of the locus created in Step 3 is a good approximation to the patch point for a non-rectilinear trajectory with a given minor-body-centered plane orientation, the major body plane orientation used in Step 2, and the angular momenta and energy used in Step 1. In other words, the displacement of the patch point caused by going from a dual rectilinear trajectory to a major-body-centered single-rectilinear trajectory is essentially identical, in magnitude and direction, to the patch point displacement caused by going from a minor-body-centered single-rectilinear trajectory to a non-rectilinear trajectory. Note that this also implies that the minor-body-centered plane passes through the minor-body-centered single-rectilinear patch point.

3.0 SPHERE OF INFLUENCE PATCH POINT EQUATION DERIVATION

3.1 Coordinate Systems

In the following analyses, two coordinate systems are used, one centered at each body. The orbital plane of the minor body is taken as the reference (xy) plane of both systems. The line joining the major and minor bodies at the time the

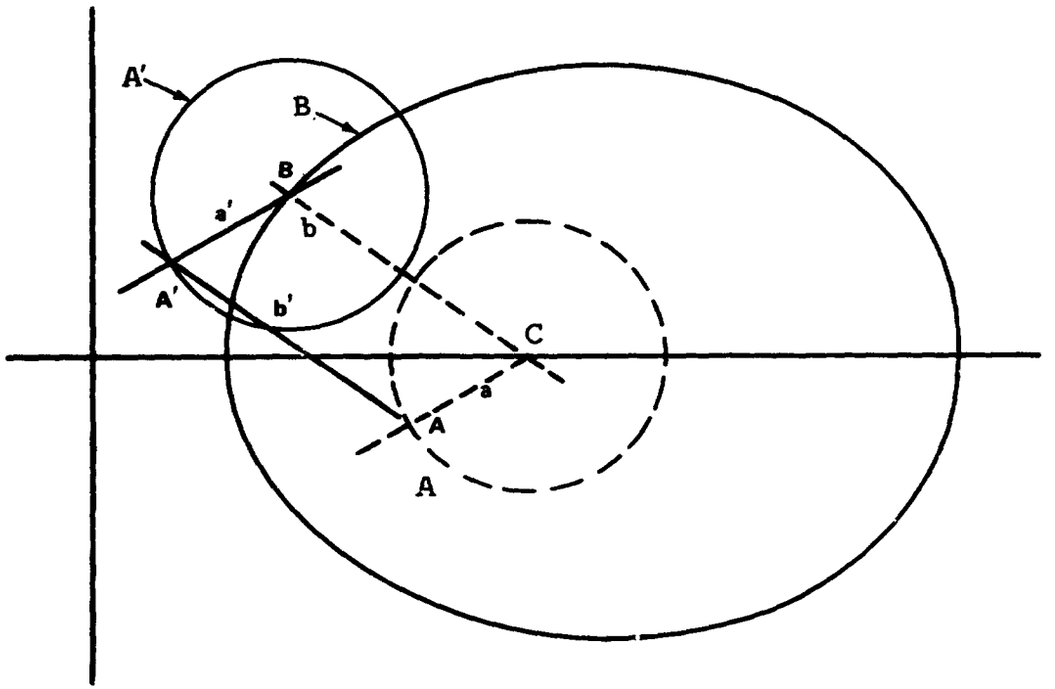

LOCI DEFINITIONS ARE THE SAME AS IN FIGURE 1 WITH THE ADDITIONS

A' – NON-RECTILINEAR PATCH POINT LOCUS
A' – NON-RECTILINEAR PATCH POINT FOR A TRAJECTORY WHOSE MINOR-BODY-CENTERED SEGMENT FORMS TRACE a' AND WHOSE MAJOR-BODY-CENTERED SEGMENT FORMS TRACE b' ON THE SPHERE OF INFLUENCE

FIGURE 2 – STRUCTURE OF THE NON-RECTILINEAR PATCH POINT POINT LOCUS

spacecraft crosses the sphere of influence is taken as the x axis for both coordinate systems. The positive x direction is taken as toward the body not at the system center. Thus, the major-body-centered positive x axis points toward the minor body and, conversely, the minor-body-centered positive x axis points toward the major body. For both coordinate systems, the positive z axis points in the same direction as the angular momentum vector of the minor body in its orbit around the major body. The positive y axis completes the right-handed triad. The transformation relationships between these systems are:

$$\left.\begin{aligned} x_1 &= -x_2 \\ y_1 &= -y_2 \\ z_1 &= +z_2 \end{aligned}\right\} \tag{1}$$

3.2 Dual Rectilinear Trajectory Patch Point

Figure 3 shows the trajectory geometry required for dual rectilinear trajectories. From the geometry of the figure, the minor-body-centered state vector at the sphere of influence is

$$\vec{R}_1 = R_1 \begin{bmatrix} \cos\lambda_{DRT}\cos\beta_{DRT} \\ \sin\lambda_{DRT}\cos\beta_{DRT} \\ \sin\beta_{DRT} \end{bmatrix} \tag{2}$$

and, since $\vec{R}_1$ and $\vec{V}_1$ are colinear,

$$\vec{V}_1 = \cdot_1 k \begin{bmatrix} \cos\lambda_{DRT}\cos\beta_{DRT} \\ \sin\lambda_{DRT}\cos\beta_{DRT} \\ \sin\beta_{DRT} \end{bmatrix} \tag{3}$$

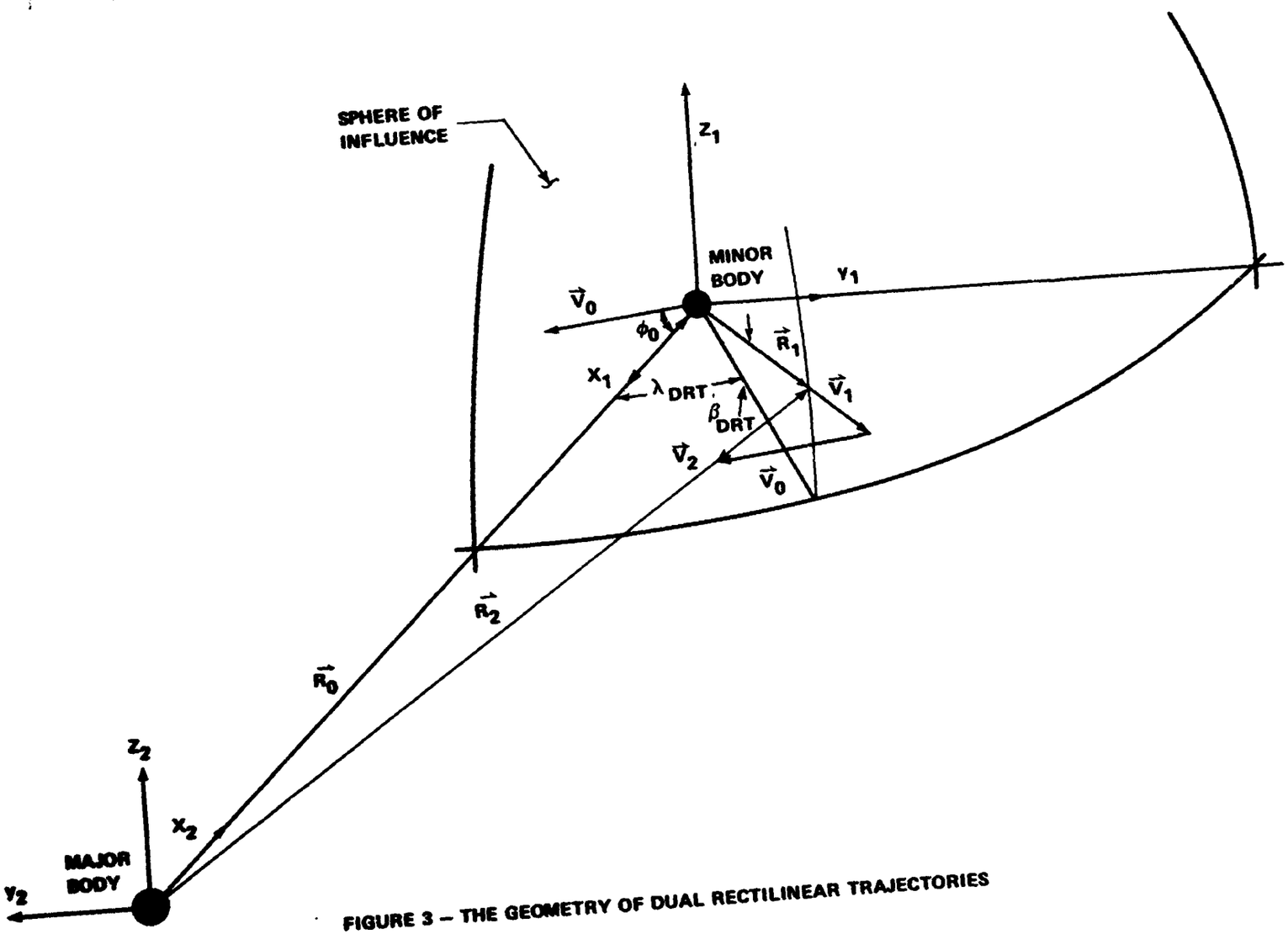

FIGURE 3 – THE GEOMETRY OF DUAL RECTILINEAR TRAJECTORIES

where k determines the direction of V_1 and obeys the following rules:

k = +1 for trajectories from the minor body to the major body.

k = -1 for trajectories from the major body to the minor body.

The major-body-centered state vector at the sphere of influence is obtained from the vector sums

$$\vec{R}_2 = \vec{R}_1 + \vec{R}_o \tag{4}$$

and

$$\vec{V}_2 = \vec{V}_1 + \vec{V}_o \tag{5}$$

where $\vec{R}_1$ and $\vec{V}_1$ must be transformed to the major body coordinate system using Eqn. (1). The state vector of the minor body referenced to the major body is given by

$$\vec{R}_o = R_o \begin{bmatrix} 1 \\ 0 \\ 0 \end{bmatrix} \tag{6}$$

and

$$\vec{V}_o = V_o \begin{bmatrix} -\cos\phi_o \\ +\sin\phi_o \\ 0 \end{bmatrix} \tag{7}$$

In order to obtain a major-body-centered rectilinear trajectory, the angular momentum with respect to the major body must be equal to zero, that is

$$\vec{R}_2 \times \vec{V}_2 = 0. \tag{8}$$

Writing Eqn. (8) in terms of Eqns. (2) through (7),

$$\begin{bmatrix} -R_1 V_o \sin\beta_{DRT} \sin\phi_o \\ -(R_1 V_o \cos\phi_o + R_o V_1 k)\ \sin\beta_{DRT} \\ R_o V_o \sin\phi_o - R_1 V_o \sin\phi_o \cos\lambda_{DRT} \cos\beta_{DRT} \\ \quad - (R_1 V_o \cos\phi_o + R_o V_1 k)\ \sin\lambda_{DRT} \cos\beta_{DRT} \end{bmatrix} = 0 \tag{9}$$

Setting the first and second components of the angular momentum equal to zero yields*

$$\sin\beta_{DRT} = 0. \tag{10}$$

That is, dual rectilinear trajectories must lie in the orbital plane of the minor body.

Setting the third component of angular momentum equal to zero (and setting $\cos\beta_{DRT} = 1$)

$$(R_1 V_o \cos\phi_o + R_o V_1 k)\sin\lambda_{DRT} + R_1 V_o \sin\phi_o \cos\lambda_{DRT} - R_o V_o \sin\phi_o = 0. \tag{11}$$

---

*An alternative solution is

$$\sin\phi_o = 0$$

and

$$V_1 k = -\frac{R_1 V_o}{R_o} \cos\phi_o$$

However, this solution is of academic interest only, since it corresponds to a rectilinear trajectory of the minor body with respect to the major body.

Equation (11) has the form

$$A\sin\alpha + B\cos\alpha + C = 0 \tag{12}$$

which can easily be solved, yielding

$$\sin\alpha = \frac{-AC \pm B\sqrt{A^2 + B^2 - C^2}}{A^2 + B^2} \quad . \tag{13}$$

We now have the equations of the dual rectilinear trajectory patch point:

$$\left.\begin{aligned} \sin\beta_{DRT} &= 0 \\ \text{and} \\ \sin\lambda_{DRT} &= \frac{-AC \pm B\sqrt{A^2 + B^2 - C^2}}{A^2 + B^2} \end{aligned}\right\} \tag{14}$$

where

$$A = R_1 V_o \cos\phi_o + R_o V_1 k$$

$$B = R_1 V_o \sin\phi_o$$

$$C = -R_o V_o \sin\phi_o \quad .$$

Thus, β_{DRT} is constant (0°) and λ_{DRT} is a function of $V_1 k$ only.

Due to the sign ambiguity on the radical, the λ_{DRT} equation yields two solutions except when

$$C^2 = A^2 + B^2 \tag{15}$$

It can be shown from purely geometrical considerations that Eqn. (15) is the condition for a major-body-centered trajectory which is tangent to the sphere of influence. Since it is not possible to have $C^2 < A^2 + B^2$ without introducing imaginary values in the λ_{DRT} equation, Eqn. (15) also imposes a lower limit on the value of V_1. Solving Eqn. (15) for V_1,

$$V_1 = - \frac{R_1 V_o \cos\phi_o + \sqrt{R_o^2 - R_1^2}\, V_o \sin\phi_o}{R_o} . \qquad (16)$$

Equation (16) represents the minimum energy for a dual rectilinear trajectory, and

$$\sin\lambda_{DRT} = - \frac{A}{C} \qquad (17)$$

is the patch point for the minimum energy trajectory. For trajectories with energies greater than that given by Eqn. (16), two values of λ_{DRT} exist, representing trajectories piercing the sphere of influence on either side of the tangent trajectory. Thus, the trajectories are grouped by

$$\text{(a)} \qquad \lambda_{DRT} < \sin^{-1}\left(-\frac{A}{C}\right)$$

or (18)

$$\text{(b)} \qquad \lambda_{DRT} > \sin^{-1}\left(-\frac{A}{C}\right)$$

The sign operating on the radical is minus for case (a) and plus for case (b). λ_{DRT} lies in the first or second quadrant for k = +1 and in the third or fourth quadrant for k = -1.

3.3 Major-Body-Centered Single-Rectilinear Trajectory Patch Point Locus

Figure 4 shows the trajectory geometry required for major-body-centered single-rectilinear trajectories. From the geometry of the figure, the minor-body-centered state vector at the sphere of influence is

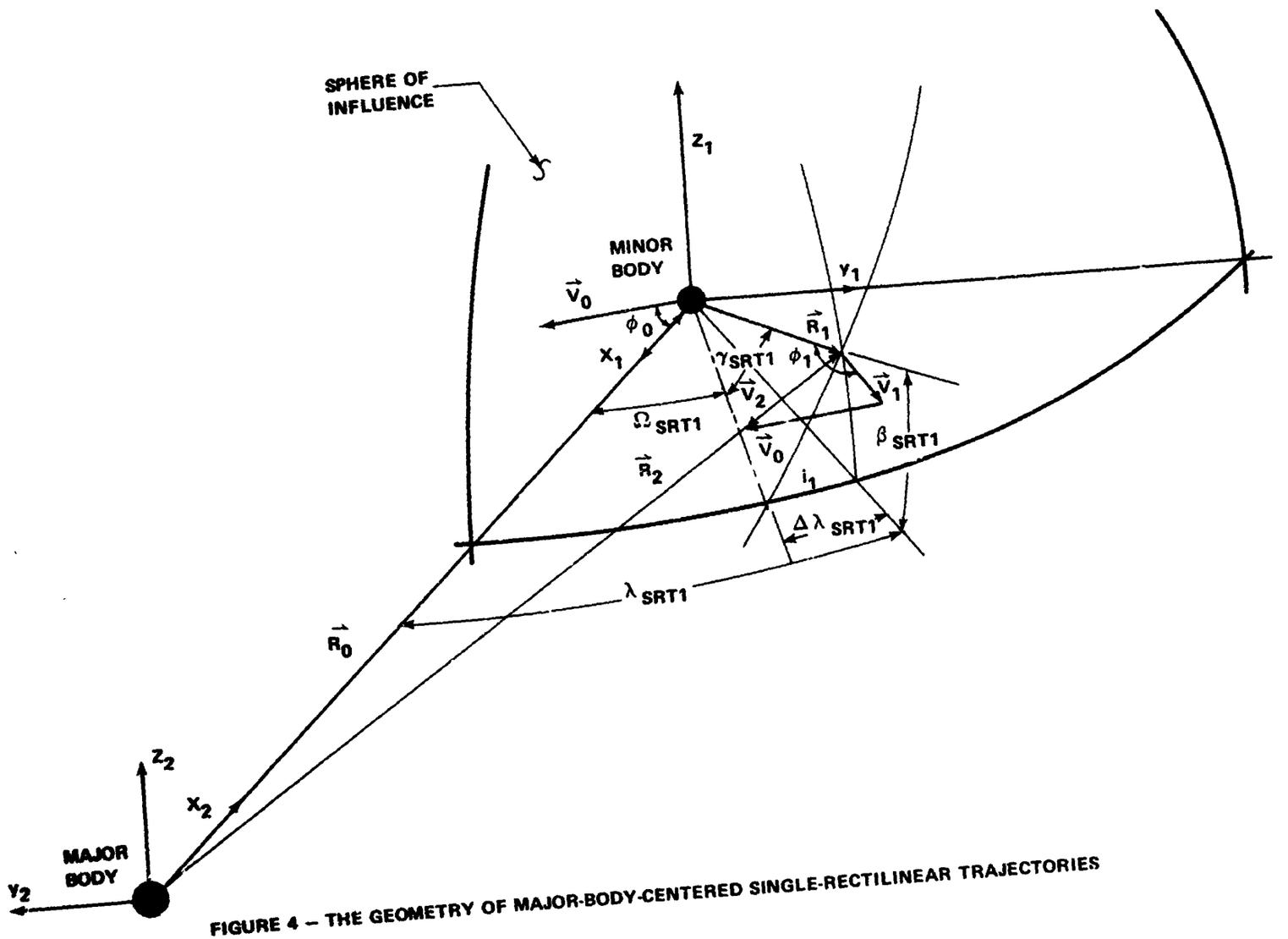

FIGURE 4 – THE GEOMETRY OF MAJOR-BODY-CENTERED SINGLE-RECTILINEAR TRAJECTORIES

$$\vec{R}_1 = R_1 \begin{bmatrix} \cos\Omega_{SRT1}\cos\gamma_{SRT1} + \sin\Omega_{SRT1}\cos i_1 \sin\gamma_{SRT1} \\ \sin\Omega_{SRT1}\cos\gamma_{SRT1} - \cos\Omega_{SRT1}\cos i_1 \sin\gamma_{SRT1} \\ \sin i_1 \sin\gamma_{SRT1} \end{bmatrix} \tag{19}$$

$$\vec{V}_1 = V_1 \begin{bmatrix} (-\cos\phi_1)(\cos\Omega_{SRT1}\cos\gamma_{SRT1} + \sin\Omega_{SRT1}\cos i_1 \sin\gamma_{SRT1}) \\ \quad + (\sin\phi_1)(\cos\Omega_{SRT1}\sin\gamma_{SRT1} - \sin\Omega_{SRT1}\cos i_1 \cos\gamma_{SRT1}) \\ (-\cos\phi_1)(\sin\Omega_{SRT1}\cos\gamma_{SRT1} - \cos\Omega_{SRT1}\cos i_1 \sin\gamma_{SRT1}) \\ \quad + (\sin\phi_1)(\sin\Omega_{SRT1}\sin\gamma_{SRT1} + \cos\Omega_{SRT1}\cos i_1 \cos\gamma_{SRT1}) \\ -\cos\phi_1 \sin i_1 \sin\gamma_{SRT1} - \sin\phi_1 \sin i_1 \cos\gamma_{SRT1} \end{bmatrix} \tag{20}$$

At this point the definitions used for inclination and node line require clarification. Three things are required to define the trajectory plane orientation: the angle between the trajectory plane and the reference plane (inclination), the location of a node, and whether this node is the ascending or descending node. The standard procedure is to select the ascending node and measure inclination as positive. However, it is convenient here to use the node line nearest the pierce point and assign an algebraic sign to the inclination to show whether this node is ascending or descending. The convention chosen is that a positive inclination should produce a positive patch point latitude for trajectories from the minor body to the major body. This convention requires i_1 to be positive if the nearest node is descending, and negative if it is ascending. The symbol Ω is used to denote the longitude of the nearest node rather than its conventional use denoting the longitude of the ascending node.

Returning to the analysis, in order to obtain a major-body-centered rectilinear trajectory, the angular momentum must equal zero, that is

$$\vec{R}_2 \times V_2 = 0. \tag{21}$$

Rewriting Eqn. (21) in terms of Eqns. (4) through (7) and Eqns. (19) and (20) yields

$$\begin{bmatrix} R_1V_1\sin\Omega_{SRT1}\sin i_1\sin\phi_1 - R_1V_o\sin i_1\sin\gamma_{SRT1}\sin\phi_o \\ - R_1V_1\cos\Omega_{SRT1}\sin i_1\sin\phi_1 - R_1V_o\sin i_1\sin\gamma_{SRT1}\cos\phi_o \\ \quad + R_oV_1(\sin i_1\sin\gamma_{SRT1}\cos\phi_1 + \sin i_1\cos\gamma_{SRT1}\sin\phi_1 \\ R_1V_1\cos i_1\sin\phi_1 \\ \quad + R_1V_o[(\sin\phi_o)(-\cos\Omega_{SRT1}\cos\gamma_{SRT1} - \sin\Omega_{SRT1}\cos i_1\sin\gamma_{SRT1}) \\ \quad + (\cos\phi_o)(-\sin\Omega_{SRT1}\cos\gamma_{SRT1} + \cos\Omega_{SRT1}\cos i_1\sin\gamma_{SRT1})] \\ \quad + R_oV_1[(\cos\phi_1)(+\sin\Omega_{SRT1}\cos\gamma_{SRT1} - \cos\Omega_{SRT1}\cos i_1\sin\gamma_{SRT1}) \\ \quad - (\sin\phi_1)(\sin\Omega_{SRT1}\sin\gamma_{SRT1} + \cos\Omega_{SRT1}\cos i_1\cos\gamma_{SRT1})] \end{bmatrix} \quad (22)$$

$$= 0$$

Setting the first component of the angular momentum equal to zero

$$\sin\gamma_{SRT1} = \frac{V_1\sin\phi_1}{V_o\sin\phi_o}\sin\Omega_{SRT1}, \quad (23)$$

which gives the patch point locus displacement from Ω_{SRT1} in terms of Ω_{SRT1}. Note that γ_{SRT1} is not a function of i_1.

Now, assuming the minor body pericenter radius is small compared to the sphere of influence radius, then $\sin\phi_1$ has a small value. If the minor body orbits the major body in a low eccentricity orbit, $\sin\phi_o$ will be approximately one.

Then, since V_o and V_1 are typically of the same order of magnitude, and since ϕ_1 grows smaller as V_1 grows larger, Eqn. (23) shows γ_{SRT1} to be a small angle. We may then make the approximations

$$\cos\phi_1 \approx -k \tag{24}$$

and

$$\cos\gamma_{SRT1} \approx 1. \tag{25}$$

Using these approximations and Eqn. (23), and setting the second component of angular momentum equal to zero, yields

$$(R_1V_o\cos\phi_o + R_oV_1k)\sin\Omega_{SRT1} + R_1V_o\sin\phi_o\cos\Omega_{SRT1} - R_oV_o\sin\phi_o = 0. \tag{26}$$

Equation (26) is identical to the dual rectilinear patch-point equation, Eqn. (11). Consequently,

$$\Omega_{SRT1} \approx \lambda_{DRT}. \tag{27}$$

Thus, it has been shown that the node line of a major-body-centered single-rectilinear trajectory is closely approximated by the path of the associated dual rectilinear trajectory. Note that this also implies that major-body-centered single-rectilinear trajectories do not exist for energies below the minimum dual rectilinear trajectory energy of Eqn. (16).

From basic spherical trigonometry relations,

$$\sin\beta_{SRT1} = \sin i_1' \sin\gamma_{SRT1} \tag{28}$$

and

$$\tan\Delta\lambda_{SRT1} = \cos i_1' \tan\gamma_{SRT1} \tag{29}$$

where $\Delta\lambda_{SRT1}$ is the longitudinal distance from Ω_{SRT1} to the single rectilinear trajectory patch point. Note that while i_1' is the trajectory plane inclination for major-body-centered single-rectilinear trajectories (and hence identical to i_1), this is no longer true when the locus is transposed to form the non-rectilinear locus, and a more general definition is required. The general definition of i_1' is the angle between the minor-body-centered trajectory plane and the plane containing the radius vector to the center of the γ_{SRT1} locus and whose line of nodes with the reference plane is perpendicular to this radius vector.

Summarizing the equations for the major-body-centered single-rectilinear patch point,

$$\left.\begin{aligned} \sin\beta_{SRT1} &= \sin i_1' \sin\gamma_{SRT1} \\ \text{and} \\ \lambda_{SRT1} &= \lambda_{DRT} + \Delta\lambda_{SRT1} \end{aligned}\right\} \qquad (30)$$

where

$$\tan\Delta\lambda_{SRT1} = \cos i_1' \tan\gamma_{SRT1}$$

and

$$\sin\gamma_{SRT1} = \frac{V_1 \sin\phi_1}{V_o \sin\phi_o} \sin\lambda_{DRT}$$

and λ_{DRT} is found from Eqn. (14). Note that i_1 carries a plus sign for trajectories whose patch point lies above the orbital plane of the minor body and a minus sign for trajectories whose patch point lies below the orbital plane of the minor body.

3.4 Minor-Body-Centered Single-Rectilinear Trajectory Patch Point Locus

Figure 5 shows the trajectory geometry required for minor-body-centered single-rectilinear trajectories. Note that

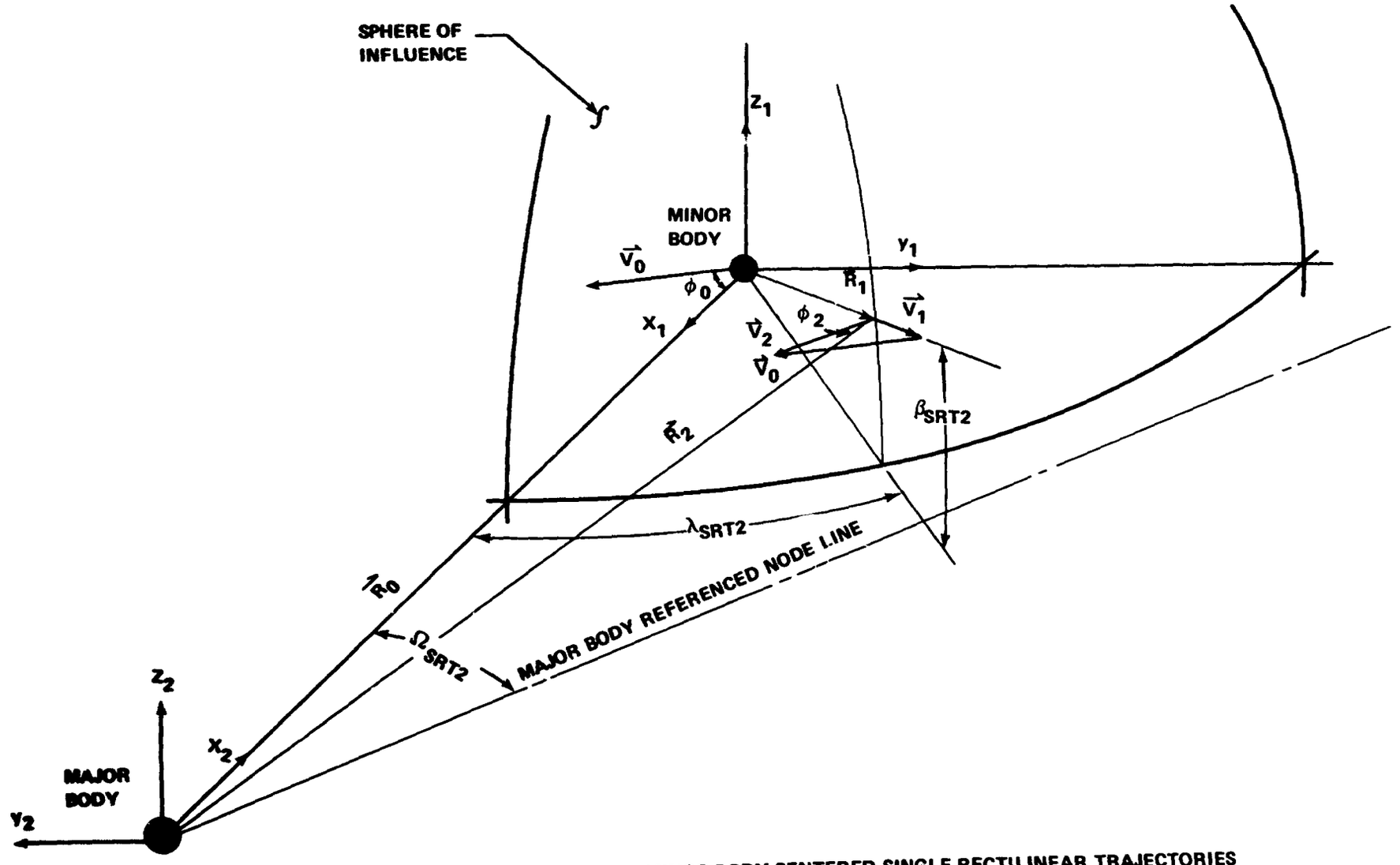

FIGURE 5 – THE GEOMETRY OF MINOR-BODY-CENTERED SINGLE-RECTILINEAR TRAJECTORIES

the state vector is defined using the patch point coordinates, since there is no defined minor-body-centered plane. From the geometry of the figure, the minor-body-centered state vector at the sphere of influence is

$$\vec{R}_1 = R_1 \begin{bmatrix} \cos\lambda_{SRT2}\cos\beta_{SRT2} \\ \sin\lambda_{SRT2}\cos\beta_{SRT2} \\ \sin\beta_{SRT2} \end{bmatrix} \tag{31}$$

and, since the minor-body-centered radius and velocity vectors are colinear,

$$\vec{V}_1 = V_1 k \begin{bmatrix} \cos\lambda_{SRT2}\cos\beta_{SRT2} \\ \sin\lambda_{SRT2}\cos\beta_{SRT2} \\ \sin\beta_{SRT2} \end{bmatrix} \tag{32}$$

where k = +1 for trajectories from the minor body to the major body

k = -1 for trajectories to the minor body from the major body.

For this case, a non-rectilinear major-body-centered trajectory is required. Hence,

$$\vec{R}_2 \times \vec{V}_2 = \vec{h}_2. \tag{33}$$

The angular momentum vector may be written

$$\vec{h}_2 = h_2 \begin{bmatrix} \sin i_2 \sin\Omega_{SRT2} \\ -\sin i_2 \cos\Omega_{SRT2} \\ \cos i_2 \end{bmatrix} \tag{34}$$

Combining Eqns. (4) through (7) and Eqns. (31) and (34)

$$\begin{bmatrix} -R_1 V_o \sin\beta_{SRT2} \sin\phi_o \\ -R_1 V_o \sin\beta_{SRT2} \cos\phi_o - R_o k V_1 \sin\beta_{SRT} \\ -R_1 V_o (\cos\lambda_{SRT2} \cos\beta_{SRT2} \sin\phi_o + \sin\lambda_{SRT2} \cos\beta_{SRT2} \cos\phi_o) \\ -R_o k V_1 \sin\lambda_{SRT2} \cos\beta_{SRT2} + R_o V_o \sin\phi_o \end{bmatrix} =$$

$$= h_2 \begin{bmatrix} \sin i_2 \sin\Omega_{SRT2} \\ -\sin i_2 \cos\Omega_{SRT2} \\ \cos i_2 \end{bmatrix} \tag{35}$$

From the first component of the angular momentum equation

$$\sin\beta_{SRT2} = - \frac{h_2 \sin i_2 \sin\Omega_{SRT2}}{R_1 V_o \sin\phi_o} \tag{36}$$

From the second component of the angular momentum equation, we find that

$$\sin\beta_{SRT2} = + \frac{h_2 \sin i_2 \cos\Omega_{SRT2}}{R_1 V_o \cos\phi_o + R_o k V_1} . \qquad (37)$$

Combining Eqns. (36) and (37)

$$\tan\Omega_{SRT2} = - \frac{R_1 V_o \sin\phi_o}{R_1 V_o \cos\phi_o + R_o k V_1} . \qquad (38)$$

Note that Ω_{SRT2} is independent of either h_2 or i_2.

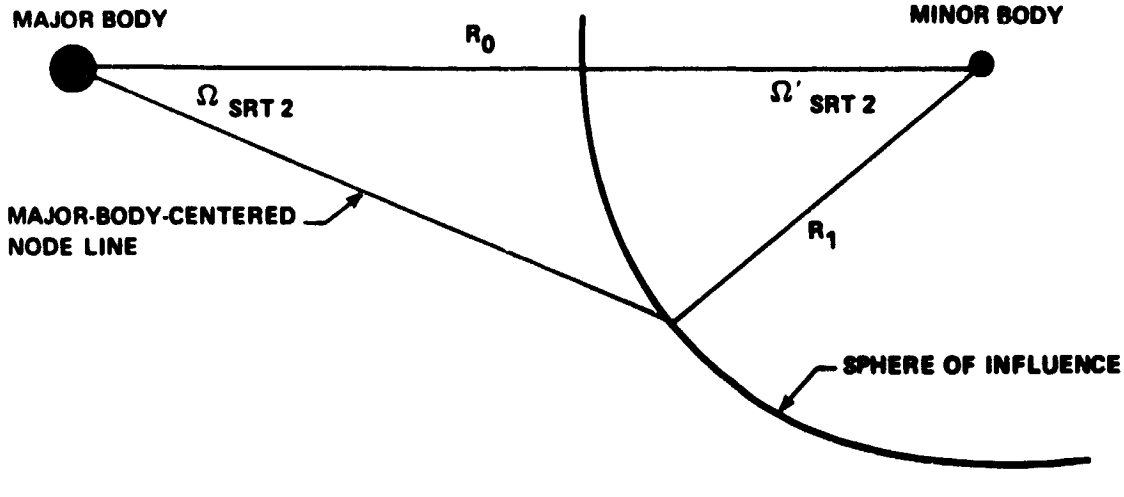

FIGURE 6 – GEOMETRY OF MINOR-BODY-CENTERED SINGLE-RECTILINEAR TRAJECTORY PLANE NODE

This being so, from Figure 6 one can write

$$\sin(\Omega_{SRT2} + \Omega'_{SRT2}) = \frac{R_o}{R_1} \sin\Omega_{SRT2} \qquad (39)$$

provided the node line intersects the sphere of influence. Combining Eqns. (38) and (39)

$$(R_o k V_1 + R_1 V_o \cos\phi_o) \sin\Omega'_{SRT2} + R_1 V_o \sin\phi_o \cos\Omega'_{SRT2} - R_o V_o \sin\phi_o = 0. \qquad (40)$$

Equation (40) is identical to the λ_{DRT} equation, Eqn. (11); hence,

$$\Omega'_{SRT2} = \lambda_{DRT}. \qquad (41)$$

Thus, it has been shown that the node line of a minor-body-centered single-rectilinear trajectory is the path of the associated dual rectilinear trajectory for energies above the minimum dual rectilinear trajectory energy. However, it is not implied in the derivation that minor-body-centered single-rectilinear trajectories do not exist for energies below this value. In fact they do exist for such energies. In these cases, the major-body-centered node line does not intersect the sphere of influence.

From the third component of the angular momentum equation

$$(R_o k V_1 + R_1 V_o \cos\phi_o) \sin\lambda_{SRT2} + R_1 V_o \sin\phi_o \cos\lambda_{SRT2} - \frac{R_o V_o \sin\phi_o - h_2 \cos i_2}{\cos\beta_{SRT2}} = 0. \qquad (42)$$

Again this is an expression of the form

$$A\sin\alpha + B\cos\alpha + C = 0$$

and Eqn. (13) constitutes the solution.

We now have the equations for the minor-body-centered single-rectilinear patch point,

$$\left.\begin{aligned} \sin\beta_{SRT2} &= -\frac{h_2 \sin i_2 \sin\Omega_{SRT2}}{R_1 V_o \sin\phi_o} \\ \tan\Omega_{SRT2} &= -\frac{R_1 V_o \sin\phi_o}{R_1 V_o \cos\phi_o + R_o k V_1} \\ \sin\lambda_{SRT2} &= -\frac{AC \pm B\sqrt{A^2 + B^2 - C^2}}{A^2 + B^2} \end{aligned}\right\} \qquad (43)$$

where

$$A = R_o k V_1 + R_1 V_o \cos\phi_o$$

$$B = R_1 V_o \sin\phi_o$$

$$C = -\frac{R_o V_o \sin\phi_o - h_2 \cos i_2}{\cos\beta_{SRT2}}$$

The angle λ_{SRT2} lies in the first or second quadrant for k = +1 and in the third or fourth quadrant for k = -1. The convention that a positive inclination produces a positive patch point latitude for minor body to major body trajectories requires a positive i_2 if the nearest node is ascending and negative i_2 if it is descending.

Because of the radical in the λ_{SRT2} equation,

$$A^2 + B^2 - C^2 = 0 \qquad (44)$$

represents a limit on minor-body-centered single-rectilinear trajectories. Solving Eqn. (44) for V_1

$$V_1 = \frac{-kR_1 V_o \cos\phi_o + \sqrt{\left(\frac{h_o - h_2 \cos i_2}{\cos\beta_{SRT1}}\right)^2 - (R_1 V_o \sin\phi_o)^2}}{R_o} \qquad (45)$$

Equation (45) imposes a lower limit on the energy of minor-body-centered single-rectilinear trajectories and

$$\sin\lambda_{SRT2} = -\frac{A}{C} \tag{46}$$

is the patch point for the minimum energy trajectory.

As before, two solutions exist for λ_{SRT2} for energy levels above that given in Eqn. (45). Both solutions are valid and are grouped by:

$$\left.\begin{array}{ll} \text{(a)} & \lambda_{SRT2} < \sin^{-1}\left[-\frac{A}{C}\right] \\ \text{or} & \\ \text{(b)} & \lambda_{SRT2} > \sin^{-1}\left[-\frac{A}{C}\right] \end{array}\right\} \tag{47}$$

The sign operating on the radical in the λ_{SRT2} equation is minus for case (a) and plus for case (b).

3.5 Non-Rectilinear Trajectory Patch Point Equations (High Energy Set)

It was stated at the beginning of the analysis that the non-rectilinear patch point locus can be obtained by properly combining the dual and single rectilinear patch point loci. Equations for these loci have now been derived, so the general locus may now be constructed. Specifically, the major-body-centered single-rectilinear patch point locus is to be transposed so that the interior point originally coinciding with the dual rectilinear patch point now lies on the minor-body-centered single-rectilinear trajectory patch point. That is,

$$\left.\begin{array}{l} \beta_{NRT} = \beta_{SRT2} + \beta_{SRT1} \\ \text{and} \\ \lambda_{NRT} = \lambda_{SRT2} + \Delta\lambda_{SRT1} \end{array}\right\} \tag{48}$$

where the values for β_{SRT1}, β_{SRT2}, $\Delta\lambda_{SRT1}$, and λ_{SRT2} are found from Eqns. (30) and (43). The value of i_1' used in Eqn. (30) must be obtained using the definition of i_1 given in Section 3.3. Spherical trigonometry easily shows that i_1' may be obtained from the true inclination, i_1, by the relationship

$$\cos i_1' = \frac{\cos i_1}{\cos \beta_{SRT1}} \tag{49}$$

An alternative method for determining β_{NRT} and λ_{NRT} is to calculate the angular distance from the minor-body-centered node line to the minor-body-centered single-rectilinear trajectory patch point and add γ_{SRT1} to this. The non-rectilinear patch point coordinates may then be calculated using this sum and i_1. The resulting equations are

$$\left.\begin{aligned} \sin\beta_{NRT} &= \sin i_1 \sin\left[\gamma_{SRT1} + \sin^{-1}\left(\frac{\sin\beta_{SRT2}}{\sin i_1}\right)\right] \\ \text{and} \\ \lambda_{NRT} &= \lambda_{SRT2} + \sin^{-1}\left(\frac{\tan\beta_{SRT2}}{\tan i_1}\right) - \sin^{-1}\left(\frac{\tan\beta_{NRT}}{\tan i_1}\right) \end{aligned}\right\} \tag{50}$$

While the two formulations give slightly different results, there does not appear to be any advantage of one over the other. Therefore, the slightly simpler Eqns. (48) are used here.

For reference purposes, Eqns. (48) will be called the high energy equation set. The reason for this selection will become apparent.

The independent parameters in the high energy equation set are:

minor-body-centered

inclination (i_1)

velocity at the sphere of influence (V_1)

trajectory flight path angle (ϕ_1)

major-body-centered

angular momentum (h_2)

inclination (i_2).

The five independent parameters and the time of piercing the sphere of influence may be considered the elements of the trajectory, just as there are five elements to Keplerian trajectories which, along with the time of pericenter passage, determine two body trajectories.

The elements V_1 and ϕ_1 may, if desired, be restated in terms of other parameters using the conic equations. For example,

$$V_1^2 = \mu_1 \left(\frac{2}{R_1} + \frac{1}{a_1} \right) \tag{51}$$

$$\sin^2 \phi_1 = \frac{\frac{R_{P1}}{R_1} \left(\frac{R_{P1}}{a_1} + 2 \right)}{\frac{R_1}{a_1} + 2} . \tag{52}$$

obtains V_1 and ϕ_1 from the semi-major axis and the radius of pericenter for the minor body. Means of obtaining h_2 are discussed in Appendix C. The parameters R_o, V_o, and ϕ_o are obtained from the minor body ephemeris and are calculated at the time the spacecraft pierces the sphere of influence.

The results of a sample trajectory problem are presented to illustrate the validity of the concepts developed

so far. Consider a trajectory from the Moon to the Earth, such as a return from an Apollo mission. The selenocentric parameters selected are:

periselene altitude	60 n. mi.
inclination	160°
semi-major axis	8×10^6 feet

and the geocentric parameters are:

inclination	30°
angular momentum	7.7×10^{11} ft^2/sec.

The radius of the Moon's sphere of influence is taken as 1.8×10^8 feet. The Moon is assumed to be at apogee, a distance of 13.34×10^8 feet from the Earth. Using standard conic orbit equations

$$V_1 = 4854.4 \text{ ft/sec}$$

and

$$\phi_1 = 176.468°.$$

The equation set gives the patch point coordinates as

$$\beta_{NRT} = 4.493°$$

$$\lambda_{NRT} = 30.803°.$$

Solving the same problem with a standard patched conic analysis, the patch point coordinates are found to be

$$\beta_{NRT} = 4.424°$$

$$\lambda_{NRT} = 30.894°$$

which agree well with the equation set calculated coordinates. Further demonstration of the validity of this equation set will be provided in Section 4.0.

As pointed out earlier, there is a lower limit on the energy of major-body-centered single-rectilinear trajectories and, consequently, on the energy for which this equation set will produce a solution. However, non-existence of these solutions does not mean that non-rectilinear trajectories do not exist at energies below this level. Indeed, many trajectories of interest do exist with energy levels below the minimum energy of major-body-centered single-rectilinear trajectories.

3.6 Non-Rectilinear Trajectory Patch Point Equations (General Set)

The energy limitation on the high energy equation set can be circumvented by eliminating the major-body-centered single-rectilinear trajectory patch point locus and deriving a new locus referenced to the minor-body-centered single-rectilinear trajectory patch point. Specifically, by assuming that the minor-body-centered trajectory plane passes through the minor-body-centered single-rectilinear trajectory patch point, it is possible to find an explicit statement for the patch point coordinates of a non-rectilinear trajectory. Since we already have the equations of the minor-body-centered single-rectilinear patch point locus, we need only obtain one more equation set. Figure 7 shows the trajectory geometry required for non-rectilinear trajectories. From the geometry of the figure, the minor-body-centered state vector at the sphere of influence can be written as

$$\dot{R}_1 = R_1 \begin{bmatrix} \cos\lambda_{SRT2}(\cos\beta_{SRT2}\cos\gamma_{NRT} - \sin\beta_{SRT2}\sin i_1' \sin\gamma_{NRT}) \\ \quad + \sin\lambda_{SRT2}\cos i_1' \sin\gamma_{NRT} \\ \sin\lambda_{SRT2}(\cos\beta_{SRT2}\cos\gamma_{NRT} - \sin\beta_{SRT2}\sin i_1' \sin\gamma_{NRT}) \\ \quad - \cos\lambda_{SRT2}\cos i_1' \sin\gamma_{NRT} \\ \sin\beta_{SRT2}\cos\gamma_{NRT} + \cos\beta_{SRT2}\sin i_1' \sin\gamma_{NRT} \end{bmatrix} \quad (53)$$

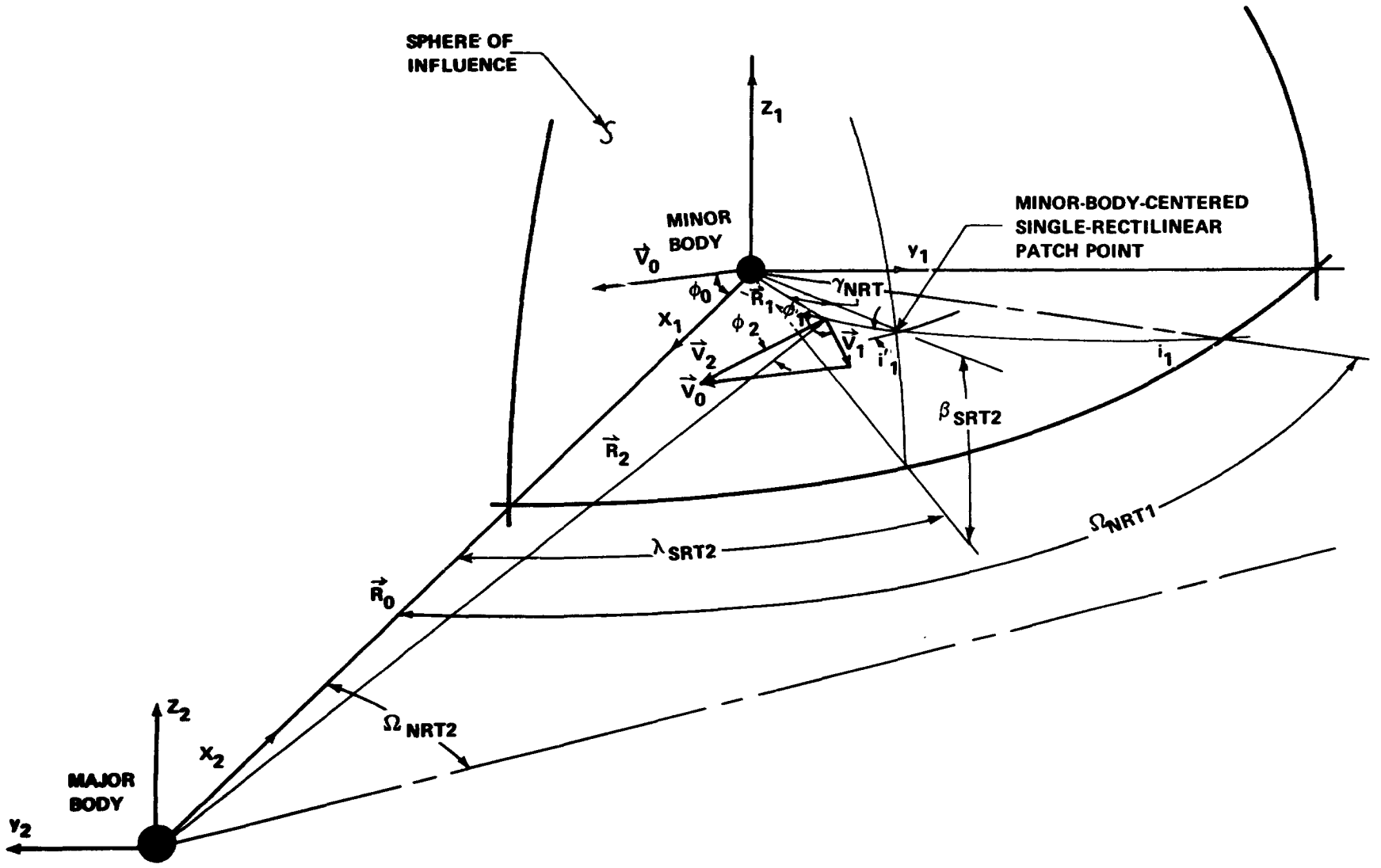

FIGURE 7 – THE GEOMETRY OF NON-RECTILINEAR TRAJECTORIES

$$\vec{V}_1 = V_1 \begin{bmatrix} [\cos\lambda_{SRT2}(\cos\beta_{SRT2}\cos\gamma_{NRT} - \sin\beta_{SRT2}\sin i_1'\sin\gamma_{NRT}) \\ \quad + \sin\lambda_{SRT2}\cos i_1'\sin\gamma_{NRT}] (-\cos\phi_1) \\ \quad + [\cos\lambda_{SRT2}(\cos\beta_{SRT2}\sin\gamma_{NRT} + \sin\beta_{SRT2}\sin i_1'\cos\gamma_{NRT}) \\ \quad - \sin\lambda_{SRT2}\cos i_1'\cos\gamma_{NRT}] (\sin\phi_1) \\ \\ [\sin\lambda_{SRT2}(\cos\beta_{SRT2}\cos\gamma_{NRT} - \sin\beta_{SRT2}\sin i_1'\sin\gamma_{NRT}) \\ \quad - \cos\lambda_{SRT2}\cos i_1'\sin\gamma_{NRT}] (-\cos\phi_1) \\ \quad + [\sin\lambda_{SRT2}(\cos\beta_{SRT2}\sin\gamma_{NRT} + \sin\beta_{SRT2}\sin i_1'\cos\gamma_{NRT}) \\ \quad + \cos\lambda_{SRT2}\cos i_1'\cos\gamma_{NRT}] (\sin\phi_1) \\ \\ [\sin\beta_{SRT2}\cos\gamma_{NRT} + \cos\beta_{SRT2}\sin i_1'\sin\gamma_{NRT}] (-\cos\phi_1) \\ \quad + [\sin\beta_{SRT2}\sin\gamma_{NRT} - \cos\beta_{SRT2}\sin i_1'\cos\gamma_{NRT}] (\sin\phi_1) \end{bmatrix} \tag{54}$$

where, from Figure 7,

$$\cos i_1' = \frac{\cos i_1}{\cos\beta_{SRT2}} \tag{55}$$

For this case, we must have

$$\vec{R}_2 \times \vec{V}_2 = \vec{h}_2. \tag{56}$$

The major-body-centered angular momentum vector may be written

$$\vec{h}_2 = h_2 \begin{bmatrix} \sin i_2 \sin\Omega_{NRT2} \\ -\sin i_2 \cos\Omega_{NRT2} \\ \cos i_2 \end{bmatrix} \tag{57}$$

The minor-body-centered angular momentum vector, expressed in the major body coordinate system, is

$$\vec{R}_1 \times \vec{V}_1 = h_1 \begin{bmatrix} -\sin i_1 \sin \Omega_{NRT1} \\ +\sin i_1 \cos \Omega_{NRT1} \\ \cos i_1 \end{bmatrix} \tag{58}$$

The angle Ω_{NRT1} may be calculated from the minor-body-centered single-rectilinear patch point as follows:

$$\Omega_{NRT1} = \lambda_{SRT2} - \sin^{-1} \left(\frac{\tan \beta_{SRT2}}{\tan i_1} \right) \tag{59}$$

Combining Eqns. (4) through (7) and Eqns. (53) through (58) yields

$$
\begin{bmatrix}
-h_1 \sin i_1 \sin\Omega_{NRT1} + R_1 V_o \sin\phi_o (\sin\beta_{SRT2} \cos\gamma_{NRT} + \cos\beta_{SRT2} \sin i_1' \sin\gamma_{NRT}) \\
\\
h_1 \sin i_1 \cos\Omega_{NRT1} - R_1 V_o \cos\phi_o (\sin\beta_{SRT2} \cos\gamma_{NRT} + \cos\beta_{SRT2} \sin i_1' \sin\gamma_{NRT}) \\
\quad + R_o V_1 \cos\phi_1 (\sin\beta_{SRT2} \cos\gamma_{NRT} + \cos\beta_{SRT2} \sin i_1' \sin\gamma_{NRT}) \\
\quad - R_o V_1 \sin\phi_1 (\sin\beta_{SRT2} \sin\gamma_{NRT} - \cos\beta_{SRT2} \sin i_1' \cos\gamma_{NRT}) \\
\\
h_1 \cos i_1 - R_1 V_o \sin\phi_o [\cos\lambda_{SRT2} (\cos\beta_{SRT2} \cos\gamma_{NRT} - \sin\beta_{SRT2} \sin i_1' \sin\gamma_{NRT}) + \sin\lambda_{SRT2} \cos i_1' \sin\gamma_{NRT}] \\
\quad - R_1 V_o \cos\phi_o [\sin\lambda_{SRT2} (\cos\beta_{SRT2} \cos\gamma_{NRT} - \sin\beta_{SRT2} \sin i_1' \sin\gamma_{NRT}) - \cos\lambda_{SRT2} \cos i_1' \sin\gamma_{NRT}] \\
\quad + R_o V_1 \cos\phi_1 [\sin\lambda_{SRT2} (\cos\beta_{SRT2} \cos\gamma_{NRT} - \sin\beta_{SRT2} \sin i_1' \sin\gamma_{NRT}) - \cos\lambda_{SRT2} \cos i_1' \sin\gamma_{NRT}] \\
\quad - R_o V_1 \sin\phi_1 [\sin\lambda_{SRT2} (\cos\beta_{SRT2} \sin\gamma_{NRT} + \sin\beta_{SRT2} \sin i_1' \cos\gamma_{NRT}) + \cos\lambda_{SRT2} \cos i_1' \cos\gamma_{NRT}] \\
\quad + R_o V_o \sin\phi_o
\end{bmatrix}
$$

$$
= \begin{bmatrix}
h_2 \sin i_2 \sin\Omega_{NRT2} \\
\\
- h_2 \sin i_2 \cos\Omega_{NRT2} \\
\\
h_2 \cos i_2
\end{bmatrix} \tag{60}
$$

Equation set (60) provides three equations with the unknown quantities γ_{NRT} and Ω_{NRT2}.

The third component of equation set (60) is a function of γ_{NRT} only. Moreover, it may be written in the form

$$A\sin\gamma_{NRT} + B\cos\gamma_{NRT} + C = 0. \tag{61}$$

Then γ_{NRT} is found, from Eqn. (13), to be

$$\sin\gamma_{NRT} = \frac{-AC \pm B\sqrt{A^2 + B^2 - C^2}}{A^2 + B^2} \tag{62}$$

where

$$\begin{aligned} A = {} & R_1V_o[(\sin\phi_o)(\cos\lambda_{SRT2}\sin\beta_{SRT2}\sin i_1' - \sin\lambda_{SRT2}\cos i_1') \\ & + (\cos\phi_o)(\sin\lambda_{SRT2}\sin\beta_{SRT2}\sin i_1' + \cos\lambda_{SRT2}\cos i_1')] \\ & + R_oV_1[(\sin\phi_1)(-\sin\lambda_{SRT2}\cos\beta_{SRT2}) \\ & + (\cos\phi_1)(-\sin\lambda_{SRT2}\sin\beta_{SRT2}\sin i_1' - \cos\lambda_{SRT2}\cos i_1')] \end{aligned}$$

$$\begin{aligned} B = {} & R_1V_o[-\sin\phi_o\cos\lambda_{SRT2}\cos\beta_{SRT2} - \cos\phi_o\sin\lambda_{SRT2}\cos\beta_{SRT2}] \\ & + R_oV_1[(\sin\phi_1)(-\sin\lambda_{SRT2}\sin\beta_{SRT2}\sin i_1' - \cos\lambda_{SRT2}\cos i_1') \\ & + \cos\phi_1\sin\lambda_{SRT2}\cos\beta_{SRT2}] \end{aligned}$$

$$C = h_1\cos i_1 - h_2\cos i_2 + R_oV_o\sin\phi_o$$

and from Eqn. (55)

$$\cos i_1' = \frac{\cos i_1}{\cos\beta_{SRT2}}$$

The quantity h_1 is found from

$$h_1 = R_1 V_1 \sin\phi_1.$$

In these equations i_1 and i_1' are signed according to the rule:

i_1 and i_1' are positive if the nearest node is descending,

i_1 and i_1' are negative if the nearest node is ascending.

Equation (62) provides two pairs of values of γ_{NRT}, the principal value and its supplement, for each choice of the sign on the radical. However, the supplementary values can be eliminated on geometrical grounds, since values of γ_{NRT} in excess of 90° would place the patch point in the wrong hemisphere. Selection of the correct value of γ_{NRT} from the two principal value solutions presents a more difficult problem. Figure 8 shows the variation of γ_{NRT} with i_1 for a typical set of a_1, h_1, i_2 and h_2 values in the Earth-Moon system. Values for $\sin\Omega_{NRT2}$ and $\cos\Omega_{NRT2}$ are obtained from the first and second components of equation set (60). Figure 9 shows the variation of the root sum square of the sine and cosine for the same parameter set used in Figure 8. It is seen that, for almost every value of i_1, only one value of γ_{NRT} satisfies the complete equation set, that is, only one value of γ_{NRT} yields a value of 1 for the root sum of the squares of the sine and cosine of Ω_{NRT2}.

However, Figure 8 shows two regions of i_1 values for which no γ_{NRT} value is available, while Figure 9 shows six discrete points for which both values of γ_{NRT} satisfy the equation set. The second of these difficulties will be dealt with first.

For a given set of a_1 i_2, and h_2 values, there are four possible minor-bodied-centered single-rectilinear patch points. These are shown in Figure 10. Tney are distinguished by the sign associated with i_2 and by the sign chosen on the

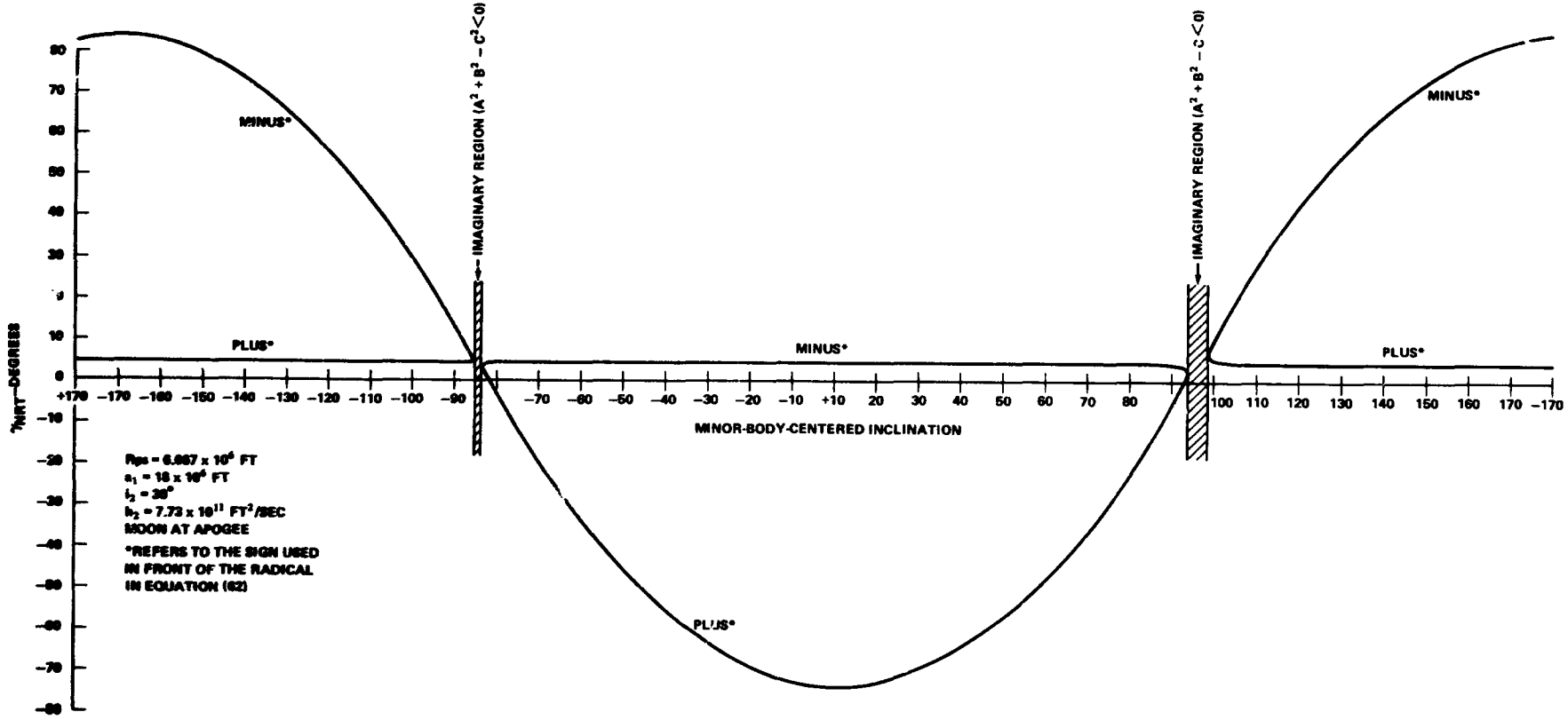

FIGURE 8 - THE VARIATION OF γ_{NRT} WITH MINOR-BODY-CENTERED INCLINATION FOR A TYPICAL EARTH-MOON TRAJECTORY

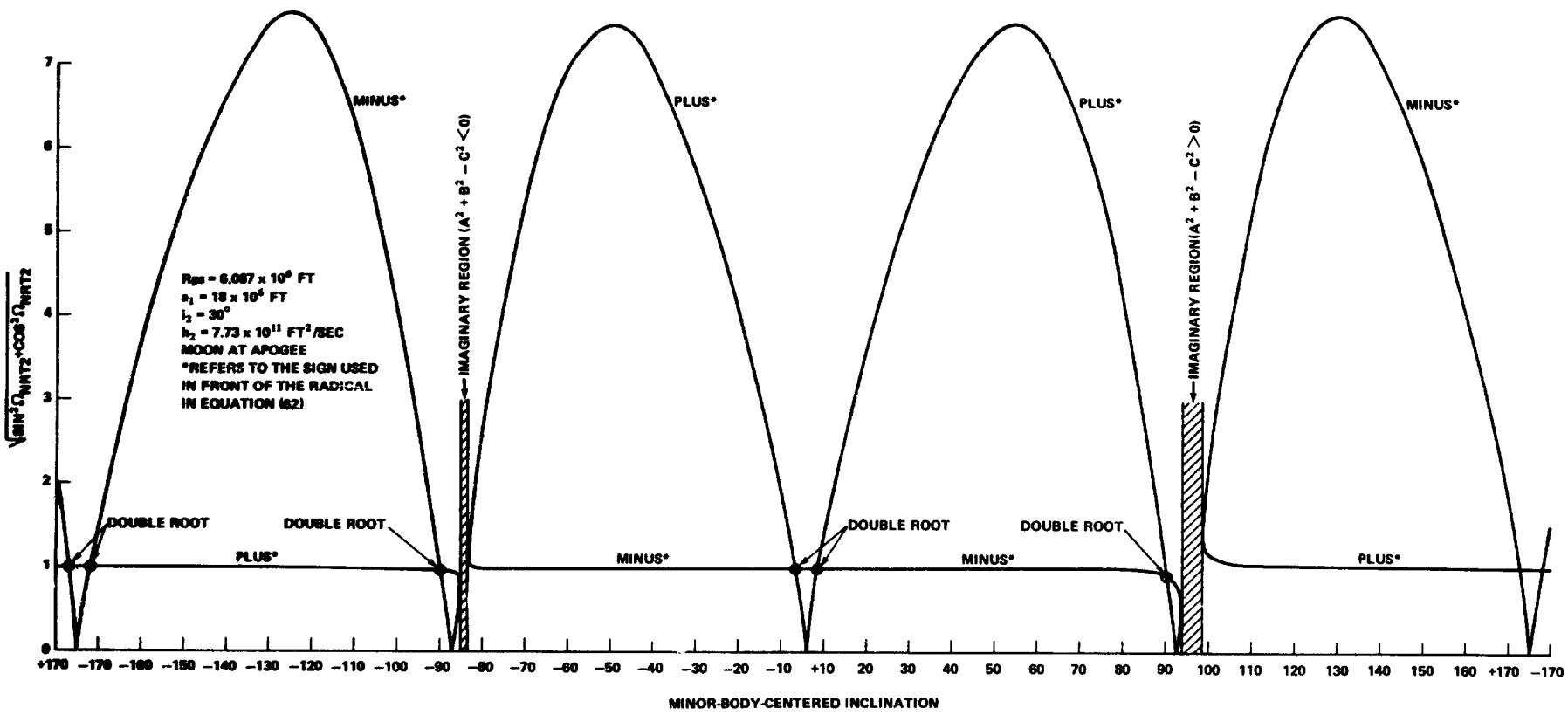

FIGURE 9 - THE VARIATION OF THE ROOT-SUM-SQUARE OF THE SINE AND COSINE OF Ω_{NRT2} WITH MINOR-BODY-CENTERED INCLINATION FOR A TYPICAL EARTH-MOON TRAJECTORY

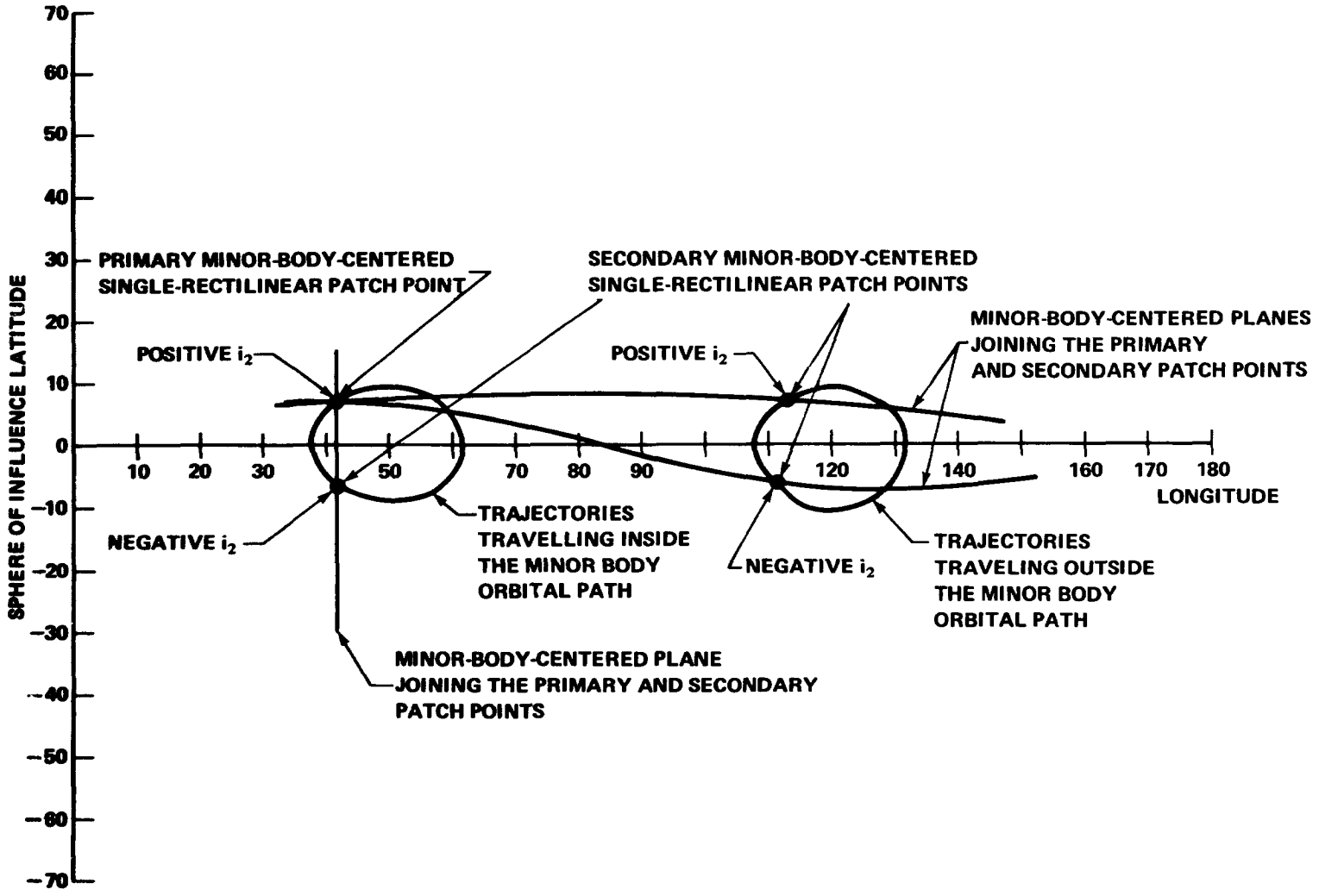

FIGURE 10 - THE PATCH POINT GEOMETRY REQUIRED FOR A DOUBLE SOLUTION TO γ_{NRT}

radical in Eqn. (43) for λ_{SRT2} (see discussion following Eqn. (45)). However, these distinctions are lost in the operations used to solve equation set (60). Now, three minor-body-centered planes may be drawn joining the primary (i.e., intended) and secondary minor-body-centered single-rectilinear patch points, also shown in Figure 10. When i_1 matches the inclination of these planes, two values of γ_{NRT} are possible and these are the two values found by Eqn. (60). There are six points with double solutions since each of the three planes may be traveled in either a retrograde or posigrade sense.

The other anomaly in Eqn. (62) is the absence of any value of γ_{NRT} for certain values of i_1. Specifically, the radical in Eqn. (62) becomes imaginary for these values of i_1. This occurs because the equations are based on the assumption that the minor-body-centered plane passes through the minor-body-centered single-rectilinear patch point. While this is a good approximation, it is not strictly true. As a result, in the region where the radical should be nearly zero, it becomes imaginary for a small range of i_1 values.

We now have, with the exceptions noted, a unique solution for γ_{NRT}. Using basic spherical trigonometry relationships,

$$\sin\Delta\beta_{NRT} = \sin i_1' \sin\gamma_{NRT} \tag{63}$$

and

$$\tan\Delta\lambda_{NRT} = \cos i_1' \tan\gamma_{NRT}. \tag{64}$$

The non-rectilinear patch point coordinates are then

$$\left.\begin{aligned} \beta_{NRT} &= \beta_{SRT2} + \Delta\beta_{NRT} \\ \text{and} \\ \lambda_{NRT} &= \lambda_{SRT2} - \Delta\lambda_{NRT}. \end{aligned}\right\} \tag{65}$$

As in the high energy equation set, an alternative formulation for the non-rectilinear patch point may be obtained by calculating the angular distance from the minor-body-centered node line to the minor-body-centered, single-rectilinear patch point, adding to this γ_{NRT} and then calculating the non-rectilinear patch point coordinates using this sum and i_1. The resulting equations are

$$\left.\begin{aligned} \sin\beta_{NRT} &= \sin i_1 \sin\left[\gamma_{NRT} + \sin^{-1}\left(\frac{\sin\beta_{SRT2}}{\sin i_1}\right)\right] \\ \text{and} \\ \lambda_{NRT} &= \lambda_{SRT2} + \sin^{-1}\left(\frac{\tan\beta_{SRT2}}{\tan i_1}\right) - \sin^{-1}\left(\frac{\tan\beta_{NRT}}{\tan i_1}\right) \end{aligned}\right\} \quad (66)$$

As there seems to be no advantage in accuracy to one formulation over the other, the simpler Eqns. (65) are used here.

Figure 11 is a plot of Eqns. (65), with the locus for a formal patched conic trajectory included for comparison. The loci are in excellent agreement except in the region where γ_{NRT} does not exist and its immediate neighborhood. In this neighborhood the locus calculated by Eqns. (65) deviates from the formally calculated patched conic locus.

From a practical calculative viewpoint, it is desirable to prevent the loci from diverging and to obtain a value for γ_{NRT} in the imaginary region. An algorithm is derived to accomplish this purpose, based on the following observations. First, the real locus is nearly symmetrical about a great circle line of inclination β_{SRT2} and passing through the minor-body-centered single-rectilinear trajectory patch point. In fact, for all but very low energies, it is nearly circular.* At the same time, when the function generated locus is misbehaving for a given value of i_1, it is usually well behaved for $-i_1$. Thus, using the symmetry of the locus, one may obtain a solution for γ_{NRT} by changing the sign on i_1.

---

*Indeed, the major-body-centered single-rectilinear trajectory locus (Eqn. (23)), used in the high energy equation set to approximate the non-rectilinear locus, is circular, since it is centered at the dual rectilinear patch point and is not a function of i_1.

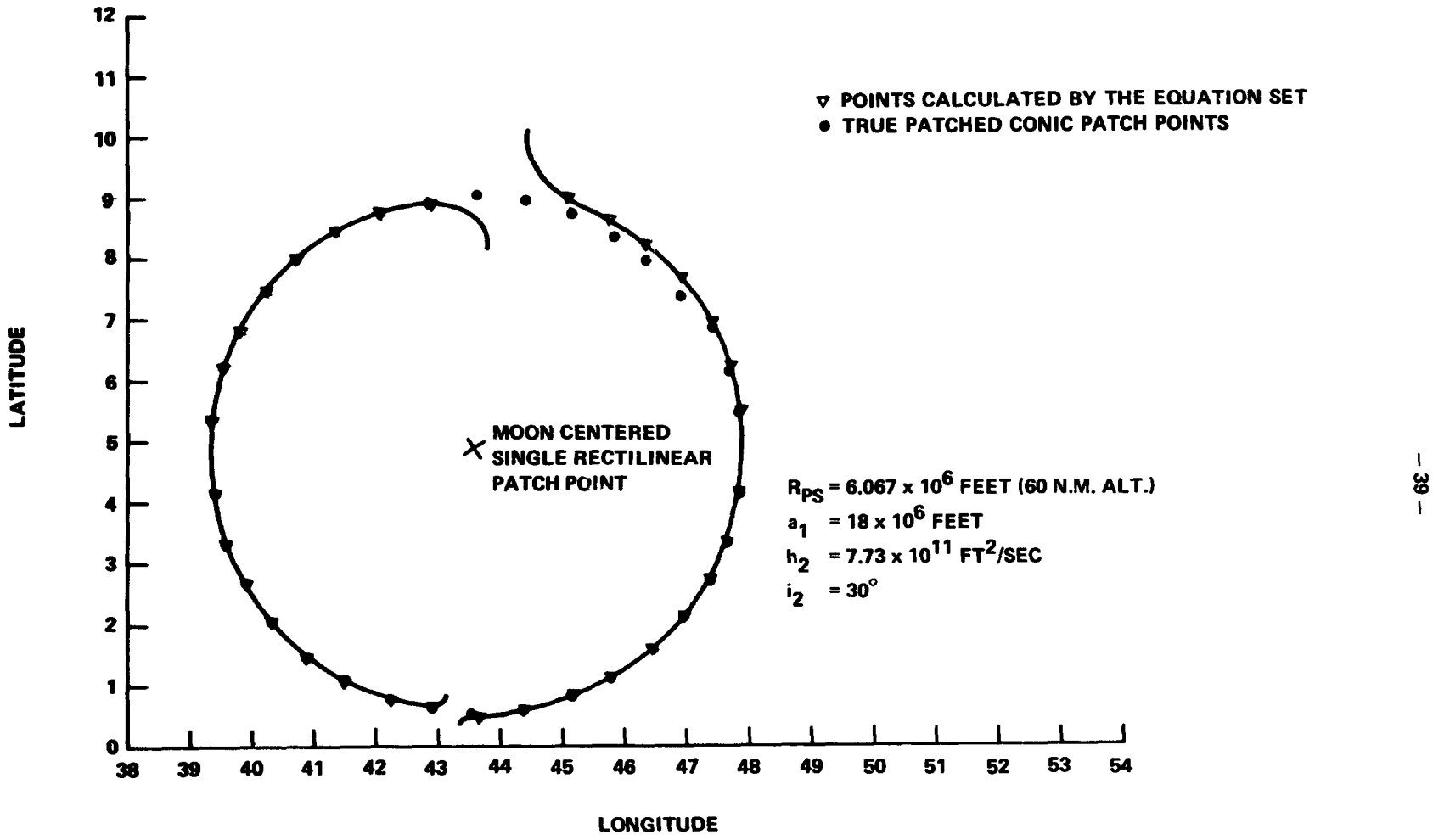

FIGURE 11 - PATCH POINT LOCUS GENERATED BY THE GENERAL EQUATION SET FOR AN EARTH-MOON TRAJECTORY

The next problem is deciding when the function is misbehaving. This always occurs when $A^2 + B^2 - C^2$ is small compared to C^2. Thus, one may make the rule that i_1 is set equal to $-i_1$ in Eqn. (73) if $A^2 + B^2 - C^2 < \varepsilon C^2$ where ε is an empirically derived small number. The author has used $\varepsilon = .01$ with success. However, this rule is not quite adequate, as the function may yield values of $A^2 + B^2 - C^2 < \varepsilon C^2$ for both $+i_1$ and $-i_1$; also, it may generate imaginary values for $\sqrt{A^2 + B^2 - C^2}$ for both i_1's. These problems can be handled as follows: if the radical is imaginary for both $+i_1$ and $-i_1$, set it equal to zero; if only one value of the radical is imaginary, use the value of i_1 that yields the real answer; and if both values of i_1 yield real answers but still $A^2 + B^2 - C^2 < \varepsilon C^2$, use the i_1 that produces the larger $A^2 + B^2 - C^2$.

Stated in algorithmic form, the above rules are:

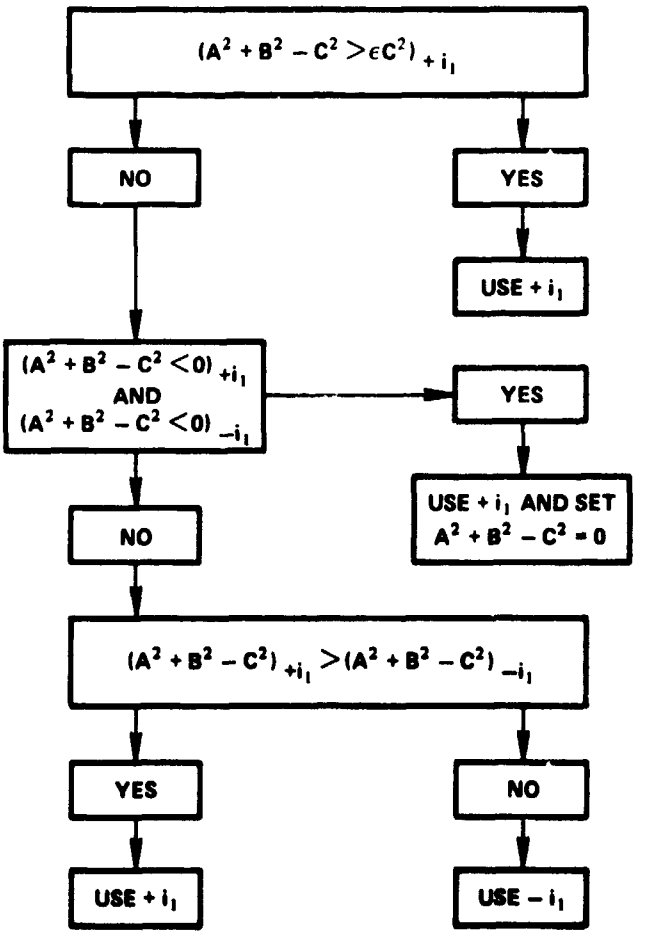

Note that the sign of i_1 is changed in Eqn. (62) only. Equations (63) and (64) use the proper value of i_1.

It is now possible to select the proper value of γ_{NRT} from the two solutions of Eqn. (62) without resorting to the γ_{NRT2} equations. Observe from Figures 8 and 9 that the proper value of γ_{NRT} is small compared with the extraneous solution. The only region where this is violated is the neighborhood of the imaginary region, but this region has been eliminated by the above algorithm. Consequently, we may simply state: the sign on the radical in Eqn. (62) is chosen to obtain the smallest positive value of γ_{NRT} for trajectories from the minor body to the major body, and the smallest negative value for trajectories from the major body to the minor body.

Figure 12 presents the same locus shown in Figure 11, incorporating the corrective algorithm given above. Also shown is the true patched conic locus. As can be seen, the locus is prevented from deviating seriously away from the path of the real locus.

The difficulties just discussed in the solution of Eqns. (70) become worse as the energy is decreased. To demonstrate that the equation set plus algorithm operates satisfactorily at very low energies, Figure 13 shows the equation set locus and the true patched conic locus for a low energy (116 hour) trip to the Moon. Comparison with the true locus shows the equation set to be producing quite good answers.

Equation (62) is limited in energy range by the minimum value of the minor-body-centered single-rectilinear trajectory energy. That is, γ_{NRT} cannot be calculated from Eqn. (62) for energies below the minimum for which a value of λ_{SRT2} exists, as given in Eqn. (45). Do such low energy trajectories exist? If so, how large is the band of energy missed by Eqn. (62)? To answer the first question, consider the nature of the derivation. Only one assumption was made, i.e., the non-rectilinear trajectory plane centered at the minor body passes through the minor-body-centered single-rectilinear patch point $(\beta_{SRT2}, \lambda_{SRT2})$. If this assumption were strictly true, then the limiting energy for λ_{SRT2} would also be the limiting energy for non-rectilinear trajectories. However, this is not the case.

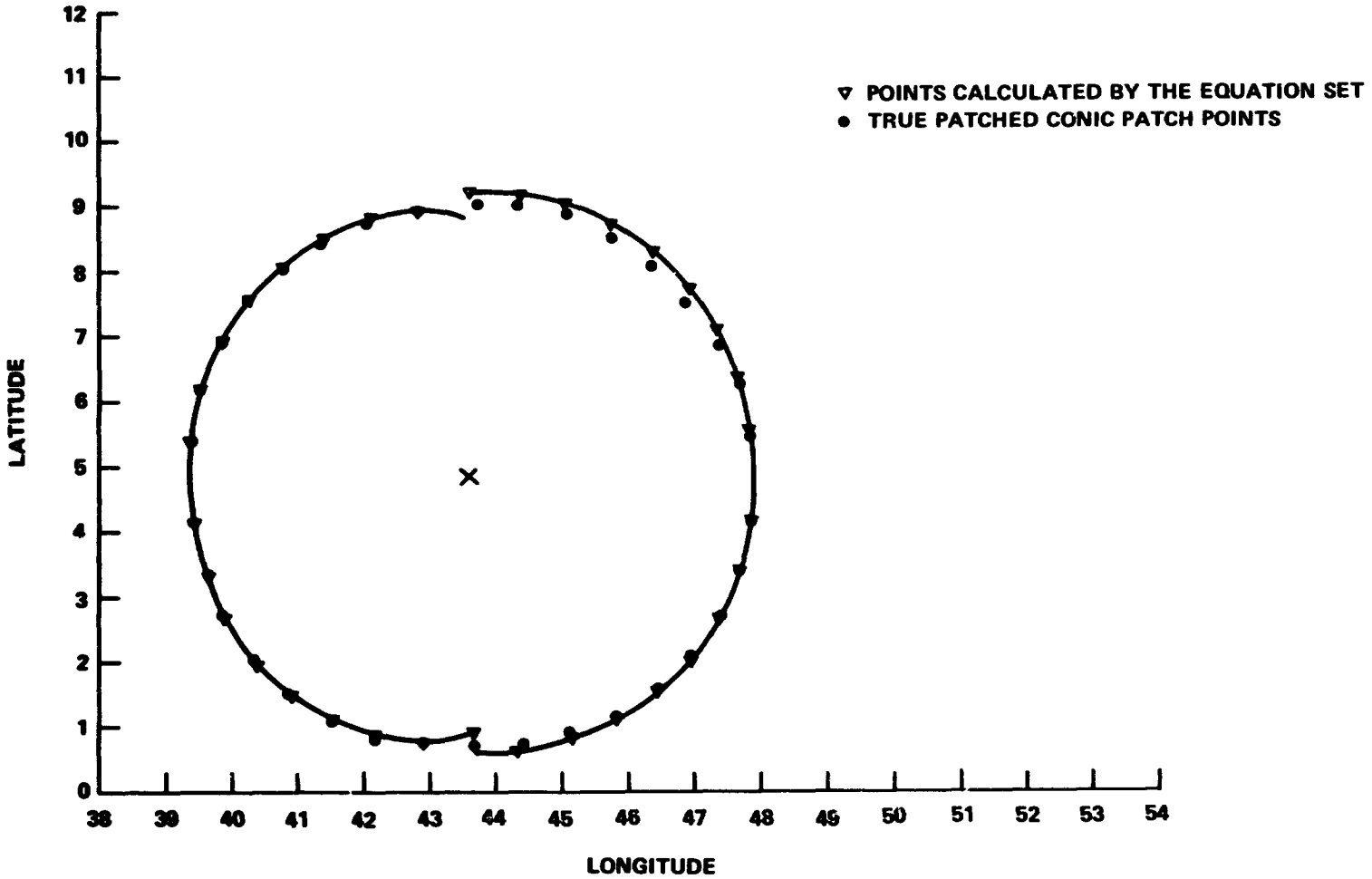

FIGURE 12 – PATCH POINT LOCUS GENERATED BY THE GENERAL EQUATION SET USING THE CORRECTIVE ALGORITHM

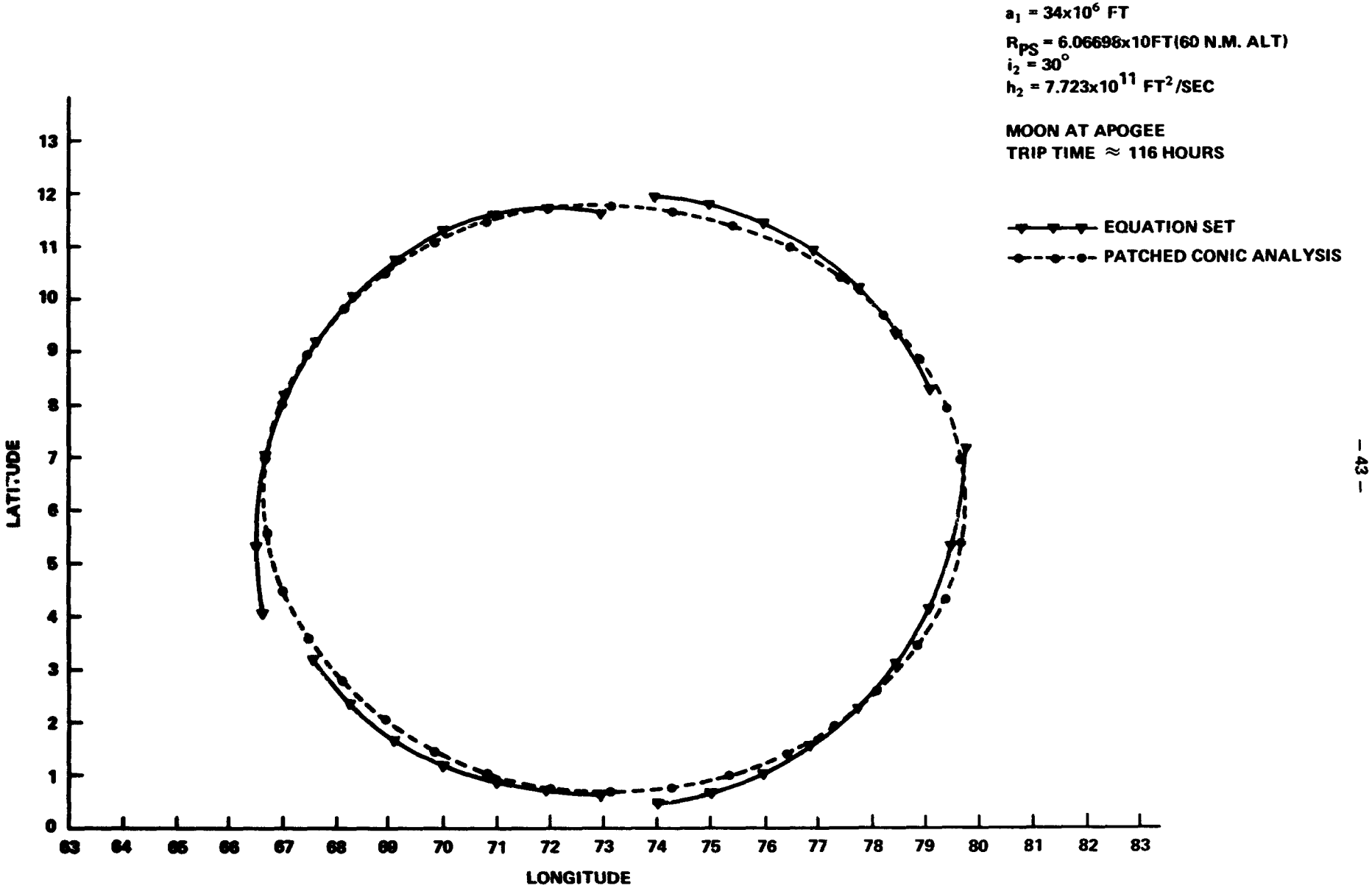

FIGURE 13 - COMPARISON OF GENERAL EQUATION SET WITH PATCHED CONIC RESULTS FOR A VERY LOW ENERGY LUNAR TRAJECTORY

Observe the case of major-body-centered, single-rectilinear trajectories. Here the associated value of λ_{SRT2} must be the dual rectilinear patch point. For this case, it was shown that the minor-body-centered plane passed through the dual rectilinear patch point, but the proof required certain approximations; thus, the result is only approximately true. Consequently, non-rectilinear trajectories may exist with energies below the minimum major-body-centered single-rectilinear trajectory energy; in fact, such trajectories do exist.

How wide a band of energy is unavailable to Eqn. (62)? Since the general equation set yields accurate results for quite low energies as demonstrated by Figure 13, one may argue that the assumption used must be fairly accurate and thus the missed energy band is quite narrow. Consider the minimum energy trajectory to the Moon (at apogee) which the general set will calculate. Take as input:

$$i_2 = 30°$$

$$h_2 = 7.72 \times 10^{11} \text{ ft}^2/\text{sec}$$

$$i_1 = 160°$$

$$R_{PS} = 6.06698 \times 10^6 \text{ ft (60 n.mi. altitude).}$$

Then the minimum energy direct trajectory has

$$a_1 = 34.8609 \times 10^6 \text{ ft}$$

and a trip time of 134 hours. Based on Apollo trajectory studies; direct trip times noticeably in excess of 134 hours do not exist. Thus, it is safe to say that the band of trajectory energies missed by Eqn. (62) is very narrow.

As in the high energy equation set, there are six trajectory elements, or independent parameters, which determine the spacecraft trajectory. They are:

minor-body-centered

inclination (i_1)

velocity at the sphere of influence (V_1)

trajectory flight path angle (ϕ_1)

major-body-centered

inclination (i_2)

angular momentum (h_2)

and the time of piercing the sphere of influence.

The elements V_1 and ϕ_1 may be restated in terms of other parameters, if desired, using the standard conic relationships. For example,

$$V_1^2 = \mu_1 \left(\frac{2}{R_1} + \frac{1}{a_1} \right) \tag{67}$$

$$\sin^2 \phi_1 = \frac{R_{P1} \left(\frac{R_{P1}}{a_1} + 2 \right)}{\frac{R_1}{a_1} + 2} . \tag{68}$$

obtains V_1 and ϕ_1 from the semi-major axis and radius of pericenter. Means of obtaining h_2 are discussed in Appendix C. R_o, V_o, and ϕ_o are determined from the minor-body ephemeris and calculated at the time the spacecraft pierces the sphere of influence.

The general equation set is valid over essentially the entire regime of possible energies. While there is a limit on the validity of the λ_{SRT2} equation, it is seen that this is not significant.

4.0 VALIDITY OF THE PATCH POINT EQUATIONS

In order to demonstrate that the techniques presented here are a good approximation to a rigorous patched conic analysis, a series of trajectory problems have been solved using a patched conic analysis, the high energy equation set, and the general equation set. The results are shown in Tables I through VI. Each table presents the results for three or four different

TABLE I

COMPARISON OF RESULTS FROM PATCH CONIC ANALYSIS AND THE HIGH ENERGY AND GENERAL EQUATION SETS FOR HIGH ENERGY LUNAR TRAJECTORIES

	SPHERE OF INFLUENCE PATCH POINT		MINOR BODY PARAMETERS			MAJOR BODY PARAMETERS	
	LATITUDE	LONGITUDE	PERI-CENTER RADIUS	INCLI-NATION	SEMI-MAJOR AXIS	ANGULAR MOMENTUM	INCLI-NATION
	DEGREES	DEGREES	FEET x 10^6	DEGREES	FEET x 10^6	$FT^2/SEC \times 10^{11}$	DEGREES
PATCH CONIC	5.000	26.000	6.0670	52.233	8.3830	7.7694	20.966
HIGH ENERGY EQN. SET	5.027	25.992	6.0670	52.233	8.3830	7.7880	21.149
GENERAL EQN. SET	5.009	25.006	6.0670	52.233	8.3830	7.7681	21.046
PATCH CONIC	5.000	32.000	6.0670	160.012	8.4097	7.7694	34.416
HIGH ENERGY EQN. SET	5.035	31.982	6.0670	160.012	8.4097	7.8069	34.580
GENERAL EQN. SET	5.038	31.991	6.0670	160.012	8.4097	7.8025	34.633
PATCH CONIC	5.000	35.000	6.0670	26.145	6.4180	7.7694	143.303
HIGH ENERGY EQN. SET	4.973	35.000	6.0670	26.145	6.4180	7.7506	143.512
GENERAL EQN. SET	4.970	35.007	6.0670	26.145	6.4180	7.7534	143.566
PATCH CONIC	5.000	40.500	6.0670	134.841	6.4655	7.7694	151.968
HIGH ENERGY EQN. SET	4.988	40.491	6.0670	134.841	6.4655	7.7551	152.039
GENERAL EQN. SET	4.990	40.493	6.0670	134.841	6.4655	7.7583	152.027

EARTH-MOON TRAJECTORIES WITH A TRIP TIME OF APPROXIMATELY 60 HOURS. THE MOON IS AT APOGEE. THE TRAJECTORY PERIGEE ALTITUDE IS 100 N.M. AND PERISELENE ALTITUDE IS 60 N.M.

TABLE II

COMPARISON OF RESULTS FROM PATCH CONIC ANALYSIS AND THE HIGH ENERGY AND GENERAL EQUATION SETS FOR INTERMEDIATE ENERGY LUNAR TRAJECTORIES

	SPHERE OF INFLUENCE PATCH POINT		MINOR BODY PARAMETERS			MAJOR BODY PARAMETERS	
	LATITUDE	LONGITUDE	PERI-CENTER RADIUS	INCLI-NATION	SEMI-MAJOR AXIS	ANGULAR MOMENTUM	INCLI-NATION
	DEGREES	DEGREES	FEET x 10^6	DEGREES	FEET x 10^6	$FT^2/SEC \times 10^{11}$	DEGREES
PATCH CONIC	6.000	40.000	6.0670	62.493	18.110	7.7373	13.612
HIGH ENERGY EQN. SET	6.139	39.959	6.0670	62.493	18.110	7.7881	14.358
GENERAL EQN. SET	6.043	40.009	6.0670	62.493	18.110	7.7421	13.865
PATCH CONIC	6.000	48.000	6.0670	161.300	18.267	7.7373	29.021
HIGH ENERGY EQN. SET	6.096	47.990	6.0670	161.300	18.267	7.7847	29.487
GENERAL EQN. SET	6.095	47.987	6.0670	161.300	18.267	7.7855	29.478
PATCH CONIC	6.000	48.000	6.0670	8.393	11.275	7.7373	127.652
HIGH ENERGY EQN. SET	5.965	47.991	6.0670	8.393	11.275	7.7117	127.783
GENERAL EQN. SET	5.967	48.011	6.0670	8.393	11.275	7.7197	127.837
PATCH CONIC	0	54.000	6.0670	94.797	10.800	7.7373	152.674
HIGH ENERGY EQN. SET	0.090	53.982	6.0670	94.797	10.800	7.7669	152.050
GENERAL EQN. SET	0.047	53.994	6.0670	94.797	10.800	7.7163	152.982

EARTH-MOON TRAJECTORIES WITH A TRIP TIME OF APPROXIMATELY 80 HOURS. THE MOON IS AT APOGEE. THE TRAJECTORY PERIGEE ALTITUDE IS 100 N.M. AND PERISELENE ALTITUDE IS 60 N.M.

TABLE III

COMPARISON OF RESULTS FROM PATCH CONIC ANALYSIS AND
THE HIGH ENERGY AND GENERAL EQUATION SETS FOR LOW ENERGY LUNAR TRAJECTORIES

	SPHERE OF INFLUENCE PATCH POINT		MINOR BODY PARAMETERS			MAJOR BODY PARAMETERS	
	LATITUDE	LONGITUDE	PERI-CENTER RADIUS	INCLI-NATION	SEMI-MAJOR AXIS	ANGULAR MOMENTUM	INCLI-NATION
	DEGREES	DEGREES	FEET x 10^6	DEGREES	FEET x 10^6	$FT^2/SEC \times 10^{11}$	DEGREES
PATCH CONIC	8.000	58.500	6.0670	44.102	22.935	7.7175	23.119
HIGH ENERGY EQN. SET				NO SOLUTION			
GENERAL EQN. SET	8.173	58.571	6.0670	44.102	22.935	7.7561	23.879
PATCH CONIC	8.000	74.500	6.0670	159.324	23.718	7.7175	31.980
HIGH ENERGY EQN. SET				NO SOLUTION			
GENERAL EQN. SET	8.475	74.766	6.0670	159.324	23.718	7.8933	33.857
PATCH CONIC	8.000	66.000	6.0670	25.367	11.389	7.7175	135.072
HIGH ENERGY EQN. SET	7.879	65.880	6.0670	25.367	11.389	7.6357	135.554
GENERAL EQN. SET	7.845	65.954	6.0670	25.367	11.389	7.6277	135.803
PATCH CONIC	8.000	77.000	6.0670	143.992	11.608	7.7175	140.265
HIGH ENERGY EQN. SET	7.931	77.204	6.0670	143.992	11.608	7.7040	140.760
GENERAL EQN. SET	7.882	77.135	6.0670	143.992	11.608	7.6742	140.982

EARTH-MOON TRAJECTORIES WITH A TRIP TIME OF APPROXIMATELY 90 HOURS. THE MOON IS AT PERIGEE. THE TRAJECTORY PERIGEE ALTITUDE IS 100 N.M. AND PERISELENE ALTITUDE IS 60 N.M.

TABLE IV

COMPARISON OF RESULTS FROM PATCH CONIC ANALYSIS AND THE
HIGH ENERGY AND GENERAL EQUATION SETS FOR MARS TRAJECTORIES

	SPHERE OF INFLUENCE PATCH POINT		MINOR BODY PARAMETERS			MAJOR BODY PARAMETERS	
	LATITUDE	LONGITUDE	PERI-CENTER RADIUS	INCLI-NATION	SEMI-MAJOR AXIS	ANGULAR MOMENTUM	INCLI-NATION
	DEGREES	DEGREES	A. U. x 10^{-5}	DEGREES	A. U. x 10^{-5}	$(A. U.)^2/DAY$	DEGREES
PATCH CONIC	0.300	–40.300	2.3463	33.903	1.9773	0.018903	0.110
HIGH ENERGY EQN. SET				NO SOLUTION			
GENERAL EQN. SET	0.297	–40.149	2.3463	33.903	1.9773	0.018903	0.111
PATCH CONIC	0.300	–41.300	2.3463	144.943	1.9815	0.018902	0.111
HIGH ENERGY EQN. SET				NO SOLUTION			
GENERAL EQN. SET	0.293	–41.145	2.3463	144.943	1.9815	0.018903	0.110
PATCH CONIC	0.300	–40.800	2.3463	89.663	1.9791	0.018903	0.154
HIGH ENERGY EQN. SET				NO SOLUTION			
GENERAL EQN. SET	0.304	–40.647	2.3463	89.633	1.9791	0.018903	0.155

EARTH-MARS TRAJECTORIES WITH A TRIP TIME OF APPROXIMATELY 245 DAYS. MARS IS AT ITS AVERAGE HELIOCENTRIC DISTANCE, THE TRAJECTORY PERIHELION RADIUS IS 1 A. U. AND THE PERICENTER ALTITUDE AT MARS IS 100 KM

TABLE V

COMPARISON OF RESULTS FROM PATCH CONIC ANALYSIS AND
THE HIGH ENERGY AND GENERAL EQUATION SETS FOR JUPITER TRAJECTORIES

	SPHERE OF INFLUENCE PATCH POINT		MINOR BODY PARAMETERS			MAJOR BODY PARAMETERS	
	LATITUDE	LONGITUDE	PERI-CENTER RADIUS	INCLI-NATION	SEMI-MAJOR AXIS	ANGULAR MOMENTUM	INCLI-NATION
	DEGREES	DEGREES	A. U.	DEGREES	A. U.	$(A.U.)^2$/DAY	DEGREES
PATCH CONIC	0.800	–64.000	.00465	33.403	0.033897	0.022370	0.559
HIGH ENERGY EQN. SET	NO SOLUTION						
GENERAL EQN. SET	1.233	–63.861	.00465	33.403	0.033897	0.022369	0.234
PATCH CONIC	0.800	–74.000	.00465	134.183	0.035344	0.022370	0.935
HIGH ENERGY EQN. SET	NO SOLUTION						
GENERAL EQN. SET	1.628	–73.725	.00465	134.183	0.035344	0.022367	0.316
PATCH CONIC	1.600	–66.000	.00465	60.829	0.034210	0.022370	0.641
HIGH ENERGY EQN. SET	NO SOLUTION						
GENERAL EQN. SET	2.347	–65.843	.00465	60.829	0.034210	0.022369	0.159
PATCH CONIC	0.600	–86.000	.00465	138.163	0.0022498	0.022370	176.334
HIGH ENERGY EQN. SET	0.634	–86.402	.00465	138.163	0.0022498	0.022390	176.242
GENERAL EQN. SET	0.846	–85.887	.00465	138.163	0.0022498	0.022388	175.659

EARTH-JUPITER TRAJECTORIES WITH A TRIP TIME OF APPROXIMATELY 945 DAYS. JUPITER IS AT APHELION, THE TRAJECTORY PERIHELION RADIUS IS 1 A.U. AND THE PERICENTER RADIUS AT JUPITER IS 500,000 N M.

TABLE VI

COMPARISON OF RESULTS FROM PATCH CONIC ANALYSIS AND THE
HIGH ENERGY AND GENERAL EQUATION SETS FOR JUPITER TRAJECTORIES

	SPHERE OF INFLUENCE PATCH POINT		MINOR BODY PARAMETERS			MAJOR BODY PARAMETERS	
	LATITUDE	LONGITUDE	PERI-CENTER RADIUS	INCLI-NATION	SEMI-MAJOR AXIS	ANGULAR MOMENTUM	INCLI-NATION
	DEGREES	DEGREES	A.U.	DEGREES	A.U.	$(A.U.)^2$/DAY	DEGREES
PATCH CONIC	0.800	–66.000	.00465	26.141	0.034783	.022366	0.333
HIGH ENERGY EQN. SET	NO SOLUTION						
GENERAL EQN. SET	1.214	–65.838	.00465	26.141	0.034783	.022366	0.078
PATCH CONIC	0.400	–66.000	.00465	25.949	0.034727	.022360	1.242
HIGH ENERGY EQN. SET	NO SOLUTION						
GENERAL EQN. SET	0.040	–65.800	.00465	25.949	0.034929	.022364	.905
PATCH CONIC	0.800	–82.000	.00465	131.892	0.036591	.022366	1.015
HIGH ENERGY EQN. SET	NO SOLUTION						
GENERAL EQN. SET	3.363	–80.916	.00465	131.892	0.036591	.022365	0.947
PATCH CONIC	(	–88.000	.00465	156.542	0.0022527	.022366	178.797
HIGH ENERGY EQN. SET	NO SOLUTION						
GENERAL EQN. SET	NO SOLUTION						

EARTH-JUPITER TRAJECTORIES WITH A TRIP TIME OF APPROXIMATELY 960 DAYS. JUPITER IS AT APHELION, THE TRAJECTORY PERIHELION RADIUS IS 1 A. U. AND THE PERICENTER RADIUS AT JUPITER IS 500,000 N. M.

trajectories, and for each trajectory, three rows of values are presented. The first row contains the results of the patched-conic analysis. These results constitute the input values for the high energy and general equation sets. The patch points calculated by the equation sets are given in the first and second columns of the last two rows in each table. These patch points should (and do) agree closely with the patched-conic patch point in the first row. Finally, the state vector obtained using the input minor-body-centered parameters and the patch points calculated by the equation sets were used to calculate the major-body-centered inclination and angular momentum. These values are presented in the last two columns of the second and third rows of each table. Again, these values should (and do) agree well with the patched conic angular momentum and inclination of the first row. The trajectory problems solved cover a range of Earth-Moon, Earth-Mars, and Earth-Jupiter trajectories. For the interplanetary trajectories, the Earth-centered trajectory portion was ignored and the trajectories were assumed to have a 1 A.U. perihelion radius.

Tables I through III cover Earth-Moon trajectories for a range of geocentric energies. The sphere of influence radius was taken as 1.8×10^8 feet for consistency with BCMASP.* Study of these tables shows that the high energy equation set produces excellent results in those cases where it is valid. However, it is not capable of calculating the patch point for low energy trajectories within the range of interest.

The results generated by the general equation set are comparable in accuracy to those from the high energy equation set. Moreover, the general set is able to calculate nearly all the trajectories unavailable from the high energy set.

Mars and Jupiter trajectory results are tabulated in Tables IV, V, and VI. For this set the radius of the sphere of influence was calculated as

$$R_1 = \left(\frac{M_{\text{minor body}}}{M_{\text{major body}}}\right)^{2/5} R_o. \qquad (69)$$

The results for Mars (Table IV) were very good. The excellence of these results comes from Mars' small sphere of influence and the small pericenter distance chosen for the problem. The results for Jupiter (Table V) are not quite as accurate. Jupiter

*Bellcomm Apollo Simulation Program.

has a large sphere of influence compared with Mars and the pericenter radius chosen for the study was also relatively large. Even so, the results are satisfactory.

Table VI shows four more trajectories from Earth to Jupiter. These have a slightly longer trip time than those in Table V and are very nearly equivalent to a Hohmann transfer. The results of the first three trajectories, which have posigrade helicentric portions, are similar to those of Table V. The last trajectory, which has a retrograde heliocentric portion, could not be calculated using either equation set.

The failure of both equation sets to calculate a patch point for this trajectory is due to the limits on the minor-body-centered single-rectilinear trajectory energy noted in Eqn. (45). The minor-body-centered energy selected is too small to give a real solution for λ_{SRT1} in Eqn. (43).

To find the real lower limit on the Jupiter trajectory energy imposed by Eqn. (45), the input value of a_1 was varied to find its minimum value for an Earth-Jupiter trajectory. The other trajectory elements selected were:

$$i_1 = 3.1°$$

$$R_{P1} = 500{,}000 \text{ n. mi.}$$

$$i_2 = 1.3°$$

$$h_2 = .02236 \text{ (A.U.)}^2/\text{day}.$$

These elements might represent a mission to Jupiter's moon Europa (Jupiter II). Jupiter was taken to be at aphelion. The minimum value for a_1 was found to be .03688 A.U. This represents a trajectory aphelion distance of 5.438 A.U. compared to Jupiter's heliocentric distance of 5.455 A.U. Thus, the heliocentric energy found is actually slightly less than the energy of a formal Hohmann transfer, so we can say that the general equation set does indeed cover essentially the entire spectrum of possible Earth-Jupiter trajectory energies.

5.0 SUMMARY

Two equation sets have been derived which provide a good approximation to the problem of patched conic analysis of

spacecraft trajectories between two large central bodies satisfying boundary conditions imposed at both central bodies. A general equation set provides solutions over essentially the entire spectrum of interesting trajectories, failing only for extremely low energy trajectories. A high energy equation set provides solutions only for the higher end of the trajectory energy spectrum; however, it is somewhat simpler than the general set. For easy reference, these equation sets are organized into a computational algorithm in Appendix B.

The primary benefit obtained from these equation sets is an exact statement of the influence of the different variables on the trajectory problem. The analyst wishing to come to grips with any problem of trajectory design is provided with a powerful tool. By using derivatives of the patch point location, problems in post-periselene abort and midcourse correction should become much more tractable. The problem of free return and planetary swingby trajectories can also be reduced to analytical form (Reference 2).

Another significant benefit is the improved calculation time for patched conic trajectories. Not only is the time on a computer reduced, but the non-iterative solution format is appropriate for use on a desk calculator if desired.

K. M. Carlson

2011-KMC-vh

K. M. Carlson

Attachments
Appendixes A, B, and C.

REFERENCES

1. Carlson, K. M., "Lunar Trajectory Geometry," Technical Memorandum TM-69-2011-3, Bellcomm, Inc., Washington, D. C., December 23, 1969.

2. Carlson, K. M., "An Analytical Solution to Swing-by Trajectories," Memorandum for File B70 12075, Bellcomm, Inc., Washington, D. C., December 28, 1970.

APPENDIX A

DEFINITIONS, SYMBOLS, AND SUBSCRIPTS

A number of terms, symbols and subscripts are utilized in the text. Definitions of frequently used terms, as well as a listing of symbols and subscripts used, are repeated here for easy reference.

A.1 Definitions

Major Body - The more massive of the two large central bodies. The gravitational field of this body is assumed to pervade all space except a spherical region about the minor body.

Minor Body - The less massive of the two large central bodies. The gravitational field of this body is assumed to act only inside its sphere of influence, a spherical region of space centered at the minor body. The radius of the sphere of influence is taken to be

$$R_1 = \left(\frac{M_{\text{minor body}}}{M_{\text{major body}}}\right)^{2/5} R_o.$$

Rectilinear Trajectory - A trajectory which rises and/or descends vertically with respect to its central body. Such trajectories have zero angular momentum.

Dual Rectilinear Trajectory - A trajectory between two central bodies in which the portions of the trajectory centered at each body are rectilinear.

Single Rectilinear Trajectory - A trajectory between two central bodies with only one rectilinear body centered portion.

Non-Rectilinear Trajectory - A trajectory which has no rectilinear portion. This is, of course, the most general case.

A.2 Symbols

a ∿ semi-major axis

h ∿ angular momentum

i ∿ inclination

i_1' ∿ modified inclination, $i_1' = \frac{\cos i_1}{\cos \beta_{SRT2}}$, taken to have the same sign as i_1

k ∿ $\begin{cases} +1 \text{ for trajectories from the minor body to the major body} \\ -1 \text{ for trajectories from the major body to the minor body} \end{cases}$

M ∿ mass

R ∿ radius

V ∿ velocity

β ∿ latitude

γ ∿ the distance the patch point is displaced from its reference point

λ ∿ longitude

μ ∿ gravitational constant of the body

ϕ ∿ the angle between the radius vector and the velocity vector, measured from the radius vector

Ω ∿ the angle between the trajectory node nearest the sphere of influence pierce point and the line between the major and minor body centers

A.3 Subscripts

DRT ∿ dual rectilinear trajectory

SRT1 ∿ major-body-centered single-rectilinear trajectory

SRT2 ∿ minor-body-centered single-rectilinear trajectory

NRT ∿ non-rectilinear trajectory

o ∿ a minor body property referenced to the major body

1 ∿ a spacecraft property referenced to the minor body and occurring at the sphere of influence

2 ∿ a spacecraft property referenced to the major body and occurring at the sphere of influence

E ∿ Earth centered

S ∿ selenocentric

A ∿ apocenter

P ∿ pericenter

AG ∿ apogee

PG ∿ perigee

PS ∿ periselene

APPENDIX B

A COMPUTATIONAL ALGORITHM FOR PATCHED CONIC TRAJECTORIES

The equation sets have been organized into an algorithmic form to facilitate their use. The required inputs are listed and the calculation described in a step by step fashion until the final solution is determined.

B.1 Basic Data Required

μ_1, μ_2 - the gravitational constants of the major and minor bodies

R_o - the distance between the major and minor body at the time of penetration of the sphere of influence

ϕ_o - the angle from the minor body radius vector to the minor body velocity vector at the time of penetration of the sphere of influence

V_o - the velocity of the minor body at the time of penetration of the sphere of influence

B.2 Trajectory Inputs

V_1 - the spacecraft minor-body-centered velocity at the sphere of influence

ϕ_1 - the spacecraft minor-body-centered flight path angle of the sphere of influence

i_1 - the spacecraft minor-body-centered inclination, referenced to the minor body's orbital plane

h_2 - the spacecraft major-body-centered angular momentum

i_2 - the spacecraft major-body-centered inclination, referenced to the minor body's orbital plane

B.3 Alternative Inputs

a_1 - the minor-body-centered semi-major axis; V_1 is obtained from

$$V_1^2 = \mu_1\left(\frac{2}{R_1} + \frac{1}{a_1}\right)$$

R_{P1} - the minor-body-centered radius of pericentron; ϕ_1 is obtained from

$$\sin^2\phi_1 = \frac{\frac{R_{P1}}{R_1}\left(\frac{R_{P1}}{a_1} + 2\right)}{\frac{R_1}{a_1} + 2}$$

R_{A2} and R_{P2} - the major-body-centered apsidal distances; h_2 is obtained from

$$h_2 = \sqrt{2\frac{\mu_2 R_{A2} R_{P2}}{R_{A2} + R_{P2}}}$$

Note that if $R_{P2} << R_{A2}$, as is typical of Earth-Moon trajectories, then

$$h_2 \approx \sqrt{2\mu_2 R_{P2}}$$

The sphere of influence radius is obtained from

$$R_1 = \left(\frac{\mu_1}{\mu_2}\right)^{2/5} R_o$$

B.4 The Minor-Body-Centered Single-Rectilinear Patch Point

$$\sin\beta_{SRT2} = - \frac{h_2 \sin i_2 \sin\Omega_{SRT2}}{R_1 V_o \sin\phi_o}$$

where

$$\tan\Omega_{SRT2} = - \frac{R_1 V_o \sin\phi_o}{R_1 V_o \cos\phi_o + R_o k V_1}$$

and

$$\sin\lambda_{SRT2} = \frac{-AC \pm B\sqrt{A^2 + B^2 - C^2}}{A^2 + B^2}$$

where

$$A = R_o k V_1 + R_1 V_o \cos\phi_o$$

$$B = R_1 V_o \sin\phi_o$$

$$C = - \frac{R_o V_o \sin\phi_o - h_2 \cos i_2}{\cos\beta_{SRT2}}$$

The angles β_{SRT2} and λ_{SRT2} are the minor-body-centered single-rectilinear patch point coordinates. The sign in the λ_{SRT2} equation is chosen according to

a) $\lambda_{SRT2} < \sin^{-1}\left(-\frac{A}{C}\right)$, use the minus sign.

b) $\lambda_{SRT2} > \sin^{-1}\left(-\frac{A}{C}\right)$, use the plus sign .

The choice of sign differentiates the minor-body-centered single-rectilinear trajectories roughly into those lying completely within the minor body's orbital path (Case a) and those that lie partly or completely outside the minor body's trajectory path (Case b). λ_{SRT2} lies in the first or second quadrant for trajectories from the minor body to the major body, and in the third or fourth quadrant for trajectories from the major body to the minor body.

B.5 The Patch Point Displacement

Next, calculate the trajectory patch point displacement from the minor-body-centered single-rectilinear patch point by either of the following two methods.

B.5.1 High Energy Trajectory Case

$$\sin\gamma_{SRT1} = \frac{V_1 \sin\phi_1}{V_o \sin\phi_o} \sin\lambda_{DRT}$$

and

$$\sin\lambda_{DRT} = \frac{-AC \pm B\sqrt{A^2 + B^2 - C^2}}{A^2 + B^2}$$

with

$$A = R_o k V_1 + R_1 V_o \cos\phi_o$$

$$B = R_1 V_o \sin\phi_o$$

$$C = -R_o V_o \sin\phi_o$$

where k determines the direction of V_1 and obeys the rules:

k = +1 for trajectories from the minor body to the major body

k = -1 for trajectories to the minor body from the major body.

The angle λ_{DRT} is the longitude of the associated dual rectilinear trajectory. The sign in the λ_{DRT} equation is chosen according to

a) if $\lambda_{DRT} < \sin^{-1}\left(-\frac{A}{C}\right)$, use the minus sign

b) if $\lambda_{DRT} > \sin^{-1}\left(-\frac{A}{C}\right)$, use the plus sign

This procedure will produce values for γ_{SRT1} only for relatively high energy trajectories. The following alternative procedure is more general.

B.5.2 General Trajectory Case

$$\sin\gamma_{NRT} = \frac{-AC \pm B\sqrt{A^2 + B^2 - C^2}}{A^2 + B^2}$$

with

$$\begin{aligned} A = {} & R_1V_o\Big[(\sin\phi_o)(\cos\lambda_{SRT2}\sin\beta_{SRT2}\sin i_1' - \sin\lambda_{SRT2}\cos i_1') \\ & + (\cos\phi_o)(\sin\lambda_{SRT2}\sin\beta_{SRT2}\sin i_1' + \cos\lambda_{SRT2}\cos i_1')\Big] \\ & + R_oV_1\Big[(\sin\phi_1)(-\sin\lambda_{SRT2}\cos\beta_{SRT2}) \\ & + (\cos\phi_1)(-\sin\lambda_{SRT2}\sin\beta_{SRT2}\sin i_1' - \cos\lambda_{SRT2}\cos i_1')\Big] \end{aligned}$$

$$\begin{aligned} B = {} & R_1V_o\Big[-\sin\phi_o\cos\lambda_{SRT2}\cos\beta_{SRT2} - \cos\phi_o\sin\lambda_{SRT2}\cos\beta_{SRT2}\Big] \\ & + R_oV_1\Big[(\sin\phi_1)(-\sin\lambda_{SRT2}\sin\beta_{SRT2}\sin i_1' - \cos\lambda_{SRT2}\cos i_1') \\ & + \cos\phi_1\sin\lambda_{SRT2}\cos\beta_{SRT2}\Big] \end{aligned}$$

$$C = h_1\cos i_1' - h_2\cos i_2 + R_oV_o\sin\phi_o$$

where

$$\cos i_1' = \frac{\cos i_1}{\cos\beta_{SRT2}},$$

and

$$h_1 = R_1 V_1 \sin\phi_1 .$$

The quantities i_1, i_1' and i_2 carry signs, according to the rules:

Nearest minor-body-centered node	
Ascending	Descending
i_1 and i_1' are negative	i_1 and i_1' are positive

and

Nearest major-body-centered node	
Ascending	Descending
i_2 is positive	i_2 is negative

Having chosen the appropriate sign for i_1 and i_1' by the above rule, this sign must be modified (for both i_1 and i_1') for use in the γ_{NRT} equation according to the following algorithm:

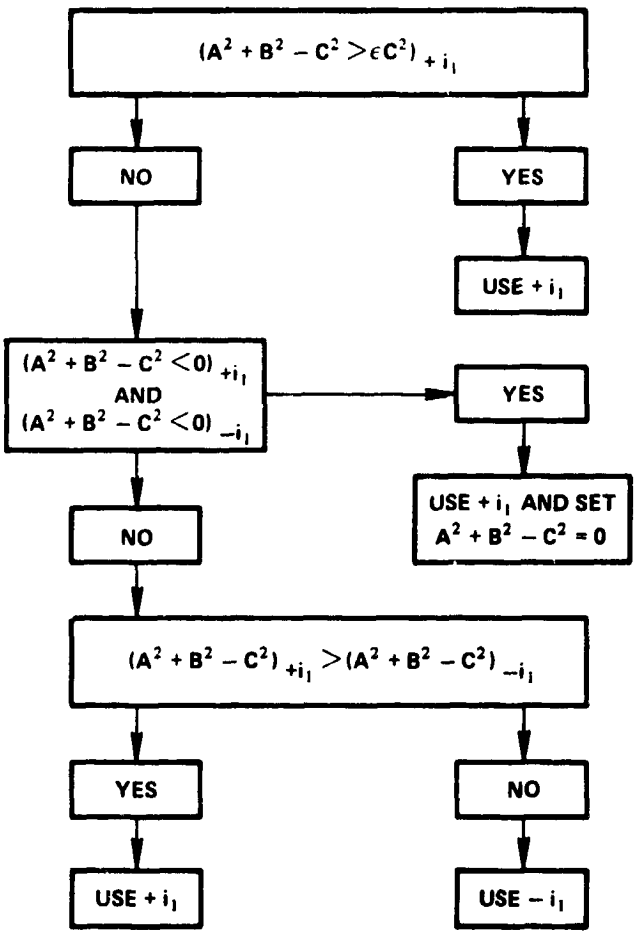

Note that the sign of i_1 is changed in the γ_{NRT} equation only. The sign on the radical in the γ_{NRT} equation is chosen to obtain the smallest positive value of γ_{NRT} for trajectories from the minor body to the major body and to obtain the smallest negative value of γ_{NRT} for trajectories from the major body to the minor body.

B.6 The Non-Rectilinear Patch Point

The non-rectilinear patch point may be obtained from the values obtained so far in either of two ways:

a) The patch point latitude is given by

$$\beta_{NRT} = \beta_{SRT2} + \Delta\beta$$

and the longitude by

$$\lambda_{NRT} = \lambda_{SRT2} - \Delta\lambda.$$

where

$$\sin\Delta\beta = \sin i_1' \sin\gamma_{SRT1}$$

$$\tan\Delta\lambda = \cos i_1' \tan\gamma_{SRT1}$$

or

$$\sin\Delta\beta = \sin i_1' \sin\gamma_{NRT}$$

$$\tan\Delta\lambda = \cos i_1' \tan\gamma_{NRT}$$

depending on whether γ_{SRT1} or γ_{NRT} was obtained in the previous step. As before

$$\cos i_1' = \frac{\cos i_1}{\cos\beta_{SRT2}}$$

b) The alternative formulation for β_{NRT}, λ_{NRT} is

$$\sin\beta_{NRT} = \sin i_1 \sin\left[\gamma_{SRT1} + \sin^{-1}\left(\frac{\sin\beta_{SRT2}}{\sin i_1}\right)\right]$$

or

$$\sin\beta_{NRT} = \sin i_1 \sin\left[\gamma_{NRT} + \sin^{-1}\left(\frac{\sin\beta_{SRT2}}{\sin i_1}\right)\right]$$

depending on whether γ_{SRT1} or γ_{NRT} was obtained in the previous step. Finally

$$\lambda_{NRT} = \lambda_{SRT2} + \sin^{-1}\left(\frac{\tan\beta_{SRT2}}{\tan i_1}\right) - \sin^{-1}\left(\frac{\tan\beta_{NRT}}{\tan i_1}\right)$$

B.7 The State Vectors at Sphere of Influence Penetration

B.7.1 The Minor-Body-Centered State Vector

The longitude of the nearest node line is

$$\Omega_1 = \lambda_{NRT} + \sin^{-1}\left(\frac{\tan\beta_{NRT}}{\tan i_1}\right)$$

The argument of latitude of the patch point with respect to Ω_2 is

$$\omega_1 = \sin^{-1}\left(\frac{\sin\beta_{NRT}}{\sin i_1}\right)$$

The position vector is then

$$x_1 = R_1(\cos\Omega_1\cos\omega_1 + \sin\Omega_1\cos i_1\sin\omega_1)$$

$$y_1 = R_1(\sin\Omega_1\cos\omega_1 - \cos\Omega_1\cos i_1\sin\omega_1)$$

$$z_1 = R_1\sin i_1\sin\omega_1$$

The velocity vector is

$$\dot{x}_1 = V_1[\sin\phi_1\ (\cos\Omega_1\sin\omega_1 - \sin\Omega_1\cos i_1\cos\omega_1) - \cos\phi_1\ (\cos\Omega_1\cos\omega_1 + \sin\Omega_1\cos i_1\sin\omega_1)]$$

$$\dot{y}_1 = V_1[\sin\phi_1\ (\sin\Omega_1\sin\omega_1 + \cos\Omega_1\cos i_1\cos\omega_1) - \cos\phi_1\ (\sin\Omega_1\cos\omega_1 - \cos\Omega_1\cos i_1\sin\omega_1)]$$

$$\dot{z}_1 = V_1[-\sin\phi_1\sin i_1\cos\omega_1 - \cos\phi_1\sin i_1\sin\omega_1]$$

B.7.2 The Major-Body-Centered State Vector

$$x_2 = R_o - x_1$$

$$y_2 = -y_1$$

$$z_2 = z_1$$

$$\dot{x}_2 = -\dot{x}_1 - V_o\cos\phi_o$$

$$\dot{y}_2 = -\dot{y}_1 + V_o\sin\phi_o$$

$$\dot{z}_2 = \dot{z}_1$$

The solution is now complete.

APPENDIX C

SOME USEFUL TECHNIQUES AND APPROXIMATIONS

C.1 Use of the Equation Sets as a Rigorous Patched-Conic Trajectory Generator

For studies that require more precise results than those available from the equation sets, these sets may be used in an iterative scheme to provide a rigorous patched-conic result. This has the advantage over standard patched-conic analyses that the iterative parameters are true trajectory parameters rather than the patch point coordinates.

To create a rigorous patched-conic result, the major-body-centered angular momentum and inclination used in the equation set become shaping parameters, and are varied until the angular momentum and inclination that are actually obtained match the desired values. A simple mirror imagining technique is effective. That is, the amount the resultant i_2 and h_2 values exceed the desired values is subtracted from the input i_2 and h_2 values. The iteration may be performed on i_2 and h_2 simultaneously. Convergence is very rapid.

C.2 Approximating the Major-Body-Centered Angular Momentum

In general, trajectory angular momentum is not one of the basic design parameters for a mission. Therefore, it would be useful to find a relationship between angular momentum and some other parameter which is basic to the mission design. For many problems of interest, this is easily done.

C.2.1 Earth-Moon Trajectories

The geocentric angular momentum may be written

$$h_E = \sqrt{\mu_E R_{PG} \left(2 - \frac{R_{PG}}{a_E}\right)} \qquad \text{(C-1)}$$

R_{PG} is typically much smaller than a_E. This can be seen by considering that $a_E = \frac{1}{2}(R_{PG} + R_{AG})$ and that $R_{AG} \geq R_o - R_1$.

Thus, the minimum a_E is $\frac{1}{2}(R_{PG} + R_o - R_1)$. Typical values for these parameters are

$$R_{PG} = .215 \times 10^8 \text{ ft (100 n. mi. altitude)}$$

$$R_o = 11.7 \times 10^8 \text{ ft (closest approach)}$$

$$R_1 = 2 \times 10^8 \text{ ft}$$

In this case R_{PG} is only 4.3% of a_E. We may then make the approximation

$$h_2 = \sqrt{2\mu_E R_{PG}}. \qquad \text{(C-2)}$$

This is the expression for the angular momentum of a parabolic trajectory with perigee radius R_{PG}. Thus, typical Earth-Moon trajectories are nearly parabolic. Normally, the perigee radius can be assumed equal to the parking orbit radius for trajectories from the Earth to the Moon. For trajectories from the Moon to the Earth which must enter the Earth's atmosphere in the Apollo entry corridor, a perigee altitude of 100,000 feet has been found to produce the desired results.

The validity of this approximation has been tested for a number of trajectories. The results are tabulated in Tables C-I to C-VIII and summarized in Table C-IX.

The data in Tables C-I to C-VIII were generated in the following steps. The title in parentheses for each step corresponds to the row name in the tables.

a) (Patched Conic) Calculate a set of trajectories using a rigorous patched-conic analysis for given values of R_{PS}, R_{PG}, geocentric energy and sphere of influence patch point coordinates.

b) (Equation Set) Calculate the patch point with the equations set, using the values of

$$a_1,\ i_1,\ R_{PS},\ i_2,\ R_{PG}$$

obtained in (a) and calculating h_E by

$$h_E = \sqrt{2\mu_E R_{PG}}$$

c) (Inverse) Use the values of geocentric energy and patch point calculated in (b), along with the values of R_{PS} and R_{PG} used in (a), to make another rigorous patched-conic analysis.

d) (Error) Take the difference between the values obtained in (a) and those obtained in (b) and (c).

Finally, the average error between (a) and (b) is calculated and stated at the bottom of each Table. The Moon's parameters were calculated from the assumed lunar elements:

$$\text{semi-major axis} = 12.54 \times 10^8 \text{ feet}$$

$$\text{eccentricity} = .06380$$

Step (c) is intended to give the analyst a feeling for the significance of the patch point errors.

Table C-IX is a listing of the average and maximum errors for each of Tables C-I to C-VIII. The results show very good agreement between techniques.

C.2.2 Interplanetary Trajectories

Another expression for angular momentum is

$$h = \sqrt{2\frac{\mu R_A R_P}{(R_A + R_P)}} \qquad \text{(C-3)}$$

where R_A is the apocenter radius and R_P is the pericenter radius. Thus, for interplanetary trajectories angular momentum is related

to the trajectory perihelion and aphelion distances. It is usually more meaningful to choose the apsidal distances rather than the angular momentum of the trajectory in mission analyses. Also, many interplanetary trajectories closely approximate the minimum energy Hohmann transfer, and for such trajectories, the heliocentric distances of the planet of departure and the planet of arrival become the apsidal distances.

TABLE C-I

TRANSLUNAR TRAJECTORIES USING THE PARABOLIC APPROXIMATION TO ANGULAR MOMENTUM
HIGH ENERGY EQUATION SET
MOON AT APOGEE; 80 HOUR TRIP TIME

	a_1	i_1	i_2	β_{NRT}	λ_{NRT}	GEOCENTRIC ENERGY
Patched Conic	0.18606×10^8	132.396	18.584	0	46.0000	-8.1700×10^6
Equation Set				−0.0836	45.9261	-8.1625×10^6
Inverse	0.18592×10^8	132.240	18.115			
Error	0.00014×10^8	0.156	0.469	0.0836	0.0739	0.0075×10^6
Patched Conic	0.18069×10^8	103.323	24.778	0	44.0000	-8.1700×10^6
Equation Set				−0.1151	43.9096	-8.1609×10^6
Inverse	0.18070×10^8	103.334	24.028			
Error	0.00001×10^8	0.011	0.750	0.1151	0.0904	0.0091×10^6
Patched Conic	0.17833×10^8	80.465	25.055	0	42.0000	-8.1700×10^6
Equation Set				−0.1260	41.8931	-8.1591×10^6
Inverse	0.17829×10^8	80.430	24.229			
Error	0.00004×10^8	0.035	0.826	0.1260	0.1069	0.0109×10^6
Patched Conic	0.18528×10^8	175.842	24.697	4.0000	48.0000	-8.1700×10^6
Equation Set				4.0986	47.9226	-8.1606×10^6
Inverse	0.18509×10^8	175.773	24.311			
Error	0.00019×10^8	0.069	0.386	0.0986	0.0774	0.0094×10^6
Patched Conic	0.18977×10^8	137.327	6.552	4.0000	46.0000	-8.1700×10^6
Equation Set				4.1439	45.9147	-8.1599×10^6
Inverse	0.18919×10^8	136.738	7.235			
Error	0.00058×10^8	0.589	0.683	0.1439	0.0853	0.0101×10^6
Patched Conic	0.18791×10^8	111 270	0.668	4.0000	44.0000	-8.1700×10^6
Equation Set				3.9990	43.8991	-8.1587×10^6
Inverse	0.18739×10^8	110.839	0.647			
Error	0.00052×10^8	0.431	0.021	0.0010	0.1009	0.0113×10^6
Patched Conic	0.17706×10^8	147.096	37.054	8.0000	48.0000	-8.1700×10^6
Equation Set				8.1590	47.8927	-8.1552×10^6
Inverse	0.17598×10^8	145.686	37.739			
Error	0.00108×10^8	1.410	0.685	0.1590	0.1073	0.0148×10^6
Patched Conic	0.18106×10^8	124.766	28.125	8.0000	46.0000	-8.1700×10^6
Equation Set				8.1792	45.8912	-8.1553×10^6
Inverse	0.17983×10^8	123.603	29.145			
Error	0.00123×10^8	1.163	1.020	0.1792	0.1098	0.0147×10^6
Patched Conic	0.18132×10^8	103.390	23.832	8.0000	44.0000	-8.1700×10^6
Equation Set				8.1859	43.8875	-8.1551×10^6
Inverse	0.18004×10^8	102.280	25.052			
Error	0.00128×10^8	1.110	1.220	0.1859	0.1125	0.0109×10^6
Patched Conic	0.14597×10^8	120.421	76.206	12.0000	50.0000	-8.1700×10^6
Equation Set				12.1189	49.9275	-8.1585×10^6
Inverse	0.14386×10^8	117.246	78.444			
Error	0.00211×10^8	3.175	2.238	0.1189	0.0725	0.0115×10^6
Patched Conic	0.15376×10^8	109.470	65.070	12.0000	48.0000	-8.1700×10^6
Equation Set				12.1284	47.9210	-8.1579×10^6
Inverse	0.15171×10^8	106.823	67.075			
Error	0.00205×10^8	2.647	2.005	0.1284	0.0790	0.0121×10^6
Patched Conic	0.15571×10^8	91.112	60.809	12.0000	46.0000	-8.1700×10^6
Equation Set				12.1160	45.9357	-8.1599×10^6
Inverse	0.15333×10^8	88.035	63.283			
Error	0.00238×10^8	3.077	2.474	0.1160	0.0643	0.0101×10^6
			AVG	0.1213	0.0900	0.0110×10^6

TABLE C-II

TRANSLUNAR TRAJECTORIES USING THE PARABOLIC APPROXIMATION TO ANGULAR MOMENTUM
HIGH ENERGY EQUATION SET
MOON ASCENDING; 75 HOUR TRIP TIME

	a_1	i_1	i_2	β_{NRT}	λ_{NRT}	GEOCENTRIC ENERGY
Patched Conic	0.17167×10^8	149.135	12.077	0	48.0000	-9.30×10^6
Equation Set				−0.0788	47.9316	-9.293×10^6
Inverse	0.17148×10^8	148.857	11.720			
Error	0.00019×10^8	0.278	0.357	0.0788	0.0684	0.0069×10^6
Patched Conic	0.16261×10^8	89.674	23.951	0	44.0000	-9.3000×10^6
Equation Set				−0.1531	43.8808	-9.2884×10^6
Inverse	0.16262×10^8	89.680	22.987			
Error	0.00001×10^8	0.006	0.964	0.1531	0.1192	0.0116×10^6
Patched Conic	0.16164×10^8	43.413	16.071	0	40.0000	-9.3000×10^6
Equation Set				−0.1214	39.8284	-9.2809×10^6
Inverse	0.16121×10^8	42.801	15.160			
Error	0.00043×10^8	0.612	0.911	0.1214	0.1716	0.0191×10^6
Patched Conic	0.16903×10^8	117.582	13.607	6.0000	46.0000	-9.3000×10^6
Equation Set				6.2199	45.8856	-9.2854×10^6
Inverse	0.16807×10^8	116.776	14.813			
Error	0.00096×10^8	0.806	1.211	0.2199	0.1144	0.0146×10^6
Patched Conic	0.16502×10^8	72.251	12.285	6.0000	42.0000	-9.3000×10^6
Equation Set				6.2035	41.8462	-9.2809×10^6
Inverse	0.16390×10^8	71.140	13.712			
Error	0.00112×10^8	1.111	1.427	0.2035	0.1538	0.0191×10^6
Patched Conic	0.12636×10^8	123.623	80.842	12.0000	52.0000	-9.3000×10^6
Equation Set				12.1275	51.9369	-9.2888×10^6
Inverse	No Inverse					
Error	Solution			0.1275	0.0631	0.0112×10^6
Patched Conic	0.14110×10^8	99.628	60.516	12.0000	48.0000	-9.3000×10^6
Equation Set				12.1458	47.9188	-9.2868×10^6
Inverse	0.13884×10^8	96.660	62.955			
Error	0.00226×10^8	2.968	2.439	0.1458	0.0812	0.0132×10^6
Patched Conic	0.95594×10^7	76.231	154.880	0	54.0000	-9.3000×10^6
Equation Set				0.1121	54.0840	-9.3074×10^6
Inverse	0.95553×10^7	76.429	155.712			
Error	0.00041×10^7	0.198	0.862	0.1121	0.0840	0.0074×10^6
Patched Conic	0.97213×10^7	53.522	143.231	2.0000	52.0000	-9.3000×10^6
Equation Set				2.0841	52.0651	-9.3054×10^6
Inverse	0.97628×10^7	55.263	141.963			
Error	0.00415×10^7	1.741	1.268	0.0841	0.0651	0.0054×10^6
			AVG	0.1385	0.1023	0.0121×10^6

TABLE C-III

TRANSLUNAR TRAJECTORIES USING THE PARABOLIC APPROXIMATION TO ANGULAR MOMENTUM
HIGH ENERGY EQUATION SET
MOON AT APOGEE; 60 HOUR TRIP TIME

	a_1	i_1	i_2	β_{NRT}	λ_{NRT}	GEOCENTRIC ENERGY
Patched Conic	0.85089×10^7	123.081	22.204	0	30.0000	-2.8000×10^6
Equation Set				−0.0210	29.9809	-2.7961×10^6
Inverse	0.85068×10^7	122.941	22.056			
Error	0.00021×10^7	0.140	0.148	0.0210	0.0191	0.0039×10^6
Patched Conic	0.84276×10^7	164.371	33.270	3.0000	32.0000	-2.8000×10^6
Equation Set				3.0216	31.9763	-2.7948×10^6
Inverse	0.84341×10^7	166.079	32.558			
Error	0.00065×10^7	1.708	0.712	0.0216	0.0237	0.0052×10^6
Patched Conic	0.86317×10^7	132.241	5.248	3.0000	30.0000	-2.8000×10^6
Equation Set				3.0388	29.9753	-2.7947×10^6
Inverse	0.86259×10^7	131.823	5.443			
Error	0.00058×10^7	0.418	0.195	0.0388	0.0247	0.0053×10^6
Patched Conic	0.85657×10^7	95.620	1.378	3.0000	28.0000	-2.8000×10^6
Equation Set				0.0333	27.9735	-2.7944×10^6
Inverse	0.85605×10^7	95.320	1.136			
Error	0.00052×10^7	0.300	0.242	0.0333	0.0265	0.0056×10^6
Patched Conic	0.75480×10^7	167.778	80.525	6.0000	36.0000	-2.8000×10^6
Equation Set				6.0558	35.9722	-2.7930×10^6
Inverse	0.75495×10^7	168.735	80.236			
Error	0.00015×10^7	0.957	0.289	0.0558	0.0287	0.0070×10^6
Patched Conic	0.79979×10^7	173.184	58.417	6.0000	34.0000	-2.8000×10^6
Equation Set				6.0472	33.9654	-2.7917×10^6
Inverse	0.79953×10^7	172.560	58.227			
Error	0.00026×10^7	0.624	0.190	0.0472	0.0346	0.0083×10^6
Patched Conic	0.83314×10^7	148.560	38.975	6.0000	32.0000	-2.8000×10^6
Equation Set				6.0501	31.9643	-2.7918×10^6
Inverse	0.83223×10^7	147.639	39.070			
Error	0.00091×10^7	0.921	0.095	0.0501	0.0357	0.0082×10^6
Patched Conic	0.84474×10^7	118.184	27.306	6.0000	30.0000	-2.8000×10^6
Equation Set				6.0505	29.9680	-2.7927×10^6
Inverse	0.84363×10^7	117.480	27.630			
Error	0.00111×10^7	0.704	0.324	0.0505	0.0320	0.0073×10^6
			AVG	0.0398	0.0279	0.0064×10^6

TABLE C-IV

TRANSLUNAR TRAJECTORIES USING THE PARABOLIC APPROXIMATION TO ANGULAR MOMENTUM
HIGH ENERGY EQUATION SET
MOON AT APOGEE; 80 HOUR TRIP TIME

	a_1	i_1	i_2	β_{NRT}	λ_{NRT}	GEOCENTRIC ENERGY
Patched Conic	0.22120×10^8	109.740	44.074	10.0000	44.0000	-8.1700×10^6
Equation Set				10.0434	43.5876	-8.1270×10^6
Inverse	0.21664×10^8	107.039	44.821			
Error	0.00456×10^8	2.701	0.757	0.0434	0.4124	0.0520×10^6
Patched Conic	0.21537×10^8	69.582	44.075	10.0000	40.0000	-8.1700×10^6
Equation Set				10.0023	39.5106	-8.1190×10^6
Inverse	0.21233×10^8	67.714	44.073			
Error	0.00304×10^8	0.232	0.003	0.0023	0.4894	0.0510×10^6
Patched Conic	0.13803×10^8	51.911	86.116	14.0000	48.0000	-8.1700×10^6
Equation Set				14.3575	48.1806	-8.1708×10^6
Inverse	0.13225×10^8	40.670	90.363			
Error	0.00578×10^8	11.241	4.247	0.3575	0.1806	0.0008×10^6
Patched Conic	0.18616×10^8	32.749	56.441	14.0000	40.0000	-8.1700×10^6
Equation Set				14.2389	39.7658	-8.1367×10^6
Inverse	0.18374×10^8	29.813	56.907			
Error	0.00242×10^8	0.064	0.466	0.2389	0.2342	0.0333×10^6
Patched Conic	0.12871×10^8	101.125	95.887	20.0000	54.0000	-8.1700×10^6
Equation Set				20.4039	54.2541	-8.1732×10^6
Inverse	No Inverse					
Error	Solution			0.4039	0.2541	0.0032×10^6
Patched Conic	0.16331×10^8	48.160	69.479	20.0000	44.0000	-8.1700×10^6
Equation Set				20.4081	44.0395	-8.1555×10^6
Inverse	0.16916×10^8	59.160	66.332			
Error	0.00585×10^8	11.000	3.147	0.4081	0.0395	0.0145×10^6
			AVG	0.2424	0.2684	0.0258×10^6

TABLE C-V

TRANSLUNAR TRAJECTORIES USING THE PARABOLIC APPROXIMATION TO ANGULAR MOMENTUM
HIGH ENERGY EQUATION SET
MOON AT APOGEE; 80 HOUR TRIP TIME

	a_1	i_1	i_2	β_{NRT}	λ_{NRT}	GEOCENTRIC ENERGY
Patched Conic	0.15186×10^8	154.571	87.655	0	−72.0000	-8.1700×10^6
Equation Set				0.9825	71.5678	-8.0956×10^6
Inverse	0.15416×10^8	157.413	82.853			
Error	0.00230×10^8	0.158	4.802	0.9825	0.4322	0.0744×10^6
Patched Conic	0.21048×10^8	169.435	22.472	0	69.0000	-8.1700×10^6
Equation Set				0.2989	68.6042	-8.1287×10^6
Inverse	0.20610×10^8	167.212	25.814			
Error	0.00438×10^8	2.223	2.342	0.2989	0.2958	0.0513×10^6
Patched Conic	0.21478×10^8	172.181	14.413	5.0000	69.0000	-8.1700×10^6
Equation Set				5.4090	68.5826	-8.1240×10^6
Inverse	0.21209×10^8	171.242	14.916			
Error	0.00269×10^8	0.939	0.503	0.4090	0.4174	0.0450×10^6
Patched Conic	0.19950×10^8	150.336	33.350	5.0000	66.5000	-8.1700×10^6
Equation Set				4.8211	66.1798	-8.1392×10^6
Inverse	0.19266×10^8	148.386	39.409			
Error	0.00684×10^8	1.950	6.059	0.1789	0.3202	0.0336×10^6
Patched Conic	0.17941×10^8	169.343	59.240	10.0000	72.0000	-8.1700×10^6
Equation Set				10.7819	70.9716	-8.0068×10^6
Inverse	0.17018×10^8	167.908	62.856			
Error	0.00923×10^8	1.435	3.616	0.7819	1.0284	0.1632×10^6
Patched Conic	0.16050×10^8	116.810	66.759	10.0000	58.4000	-8.1700×10^6
Equation Set				9.7810	58.1513	-8.1364×10^6
Inverse	No Inverse					
Error				0.2190	0.2487	0.0308×10^6
Patched Conic	0.20726×10^8	144.973	19.262	15.0000	65.0000	-8.1700×10^6
Equation Set				15.8146	64.2683	-8.0784×10^6
Inverse	0.20046×10^8	143.942	23.235			
Error	0.00680×10^8	1.031	3.973	0.8146	0.7317	0.0916×10^6
Patched Conic	0.14693×10^8	143.782	92.059	20.0000	71.0000	-8.1700×10^6
Equation Set				20.6139	69.6557	-8.0008×10^6
Inverse	0.13539×10^8	140.093	102.1224			
Error	0.01154×10^8	3.689	10.063	0.6139	1.3443	0.1692×10^6
Patched Conic	0.20047×10^8	121.511	13.585	20.0000	57.0000	-8.1700×10^6
Equation Set				20.8720	56.2725	-8.0774×10^6
Inverse	0.19404×10^8	120.633	18.519			
Error	0.00643×10^8	0.878	4.934	0.8720	0.7274	0.0926×10^6
Patched Conic	0.11248×10^8	97.537	140.941	25.0000	57.0000	-8.1700×10^6
Equation Set				24.4829	56.5375	-8.1286×10^6
Inverse	0.11046×10^8	96.542	145.441			
Error	0.00202×10^8	0.995	4.500	0.5171	0.1625	0.0414×10^6
			AVG	0.9688	0.5709	0.0793×10^6

TABLE C-VI

TRANSLUNAR TRAJECTORIES USING THE PARABOLIC APPROXIMATION TO ANGULAR MOMENTUM

HIGH ENERGY EQUATION SET

MOON AT APOGEE; 80 HOUR TRIP TIME

	a_1	i_1	i_2	β_{NRT}	λ_{NRT}	GEOCENTRIC ENERGY
Patched Conic	0.21501×10^8	111.348	51.354	4.0000	54.0000	-8.1700×10^6
Equation Set				4.3792	53.8165	-8.1683×10^6
Inverse	0.22247×10^8	112.275	48.533			
Error	0.00746	0.927	2.821	0.3792	0.1835	0.0017×10^6
Patched Conic	0.18270×10^8	93.661	61.484	4.0000	48.0000	-8.1700×10^6
Equation Set				4.1258	47.3723	-8.1141×10^6
Inverse	0.18202×10^8	93.539	60.675			
Error	0.00068×10^8	0.122	0.809	0.1258	0.6277	0.0559×10^6
Patched Conic	0.22034×10^8	100.692	46.322	6.0000	48.0000	-8.1700×10^6
Equation Set				7.0660	47.5005	-8.1568×10^6
Inverse	0.23301×10^8	102.050	41.134			
Error	0.01267×10^8	1.358	5.188	1.0660	0.4995	0.0132×10^6
Patched Conic	0.21039×10^8	91.465	47.984	6.0000	44.0000	-8.1700×10^6
Equation Set				6.8737	43.1564	-8.1134×10^6
Inverse	0.21706×10^8	92.306	43.882			
Error	0.00667×10^8	0.841	4.102	0.8737	0.8436	0.0566×10^6
Patched Conic	0.85754×10^7	57.918	159.124	12.0000	48.0000	-8.1700×10^6
Equation Set				11.0533	47.9265	-8.1397×10^6
Inverse	0.86579×10^7	58.805	154.265			
Error	0.00825×10^7	0.887	4.859	0.9467	0.0735	0.0303×10^6
Patched Conic	0.81972×10^7	28.021	167.410	12.0000	40.0000	-8.1700×10^6
Equation Set				11.6782	40.2808	-8.2026×10^6
Inverse	0.82075×10^7	28.284	169.273			
Error	0.00103×10^7	0.263	1.863	0.3218	0.2808	0.0326×10^6
Patched Conic	0.87779×10^7	74.928	160.089	24.0000	54.0000	-8.1700×10^6
Equation Set				23.1392	54.5368	-8.2361×10^6
Inverse	0.87744×10^7	74.893	163.885			
Error	0.00035×10^7	0.035	3.796	0.8608	0.5368	0.0661×10^6
Patched Conic	0.93289×10^7	43.986	131.307	24.0000	40.0000	-8.1700×10^6
Equation Set				23.7883	41.1382	-8.3020×10^6
Inverse	0.93618×10^7	44.477	133.776			
Error	0.00329×10^7	0.491	2.469	0.2117	1.1382	0.1320×10^6
Patched Conic	0.12203×10^8	88.743	101.872	36.0000	54.0000	-8.1700×10^6
Equation Set				35.8902	54.0564	-8.1316×10^6
Inverse	0.12118×10^8	88.441	102.832			
Error	0.00085×10^8	0.302	0.960	0.1098	0.0564	0.0116×10^6
Patched Conic	0.14466×10^8	69.777	79.386	36.0000	40.0000	-8.1700×10^6
Equation Set				36.3200	40.8693	-8.2539×10^6
Inverse	0.14773×10^8	70.734	78.974			
Error	0.00307×10^8	0.957	0.412	0.3200	0.8693	0.0839×10^6
			AVG	0.5216	0.5109	0.0484×10^6

TABLE C-VII

TRANSLUNAR TRAJECTORIES USING THE PARABOLIC APPROXIMATION TO ANGULAR MOMENTUM

GENERAL EQUATION SET

MOON ASCENDING; 75 HOUR TRIP TIME

	a_1	i_1	i_2	β_{NRT}	λ_{NRT}	GEOCENTRIC ENERGY
Patched Conic	0.17167×10^8	149.135	12.077	0	48.0000	-9.3000×10^6
Equation Set				0.0494	47.8820	-9.2875
Inverse	0.17116×10^8	148.409	12.050			
Error	0.00051×10^8	0.726	0.027	0.0494	0.1180	0.0125×10^6
Patched Conic	0.16261×10^8	89.674	23.951	0	44.0000	-9.3000×10^6
Equation Set				0.3429	43.8836	-9.2826×10^6
Inverse	0.16088×10^8	88.095	26.132			
Error	0.00173×10^8	1.579	2.181	0.3429	0.1164	0.0174×10^6
Patched Conic	0.16164×10^8	43.413	16.071	0	40.0000	-9.3000×10^6
Equation Set				0.0692	39.8839	-9.2870×10^6
Inverse	0.16110×10^8	42.514	16.207			
Error	0.00054×10^8	0.899	0.136	0.0692	0.1161	0.0130×10^6
Patched Conic	0.16903×10^8	117.582	13.607	6.0000	46.0000	-9.3000×10^6
Equation Set				6.2327	45.8924	-9.2860×10^6
Inverse	0.16808×10^8	116.780	14.894			
Error	0.00095×10^8	0.802	1.287	0.2327	0.1076	0.0140×10^6
Patched Conic	0.16502×10^8	72.251	12.285	6.0000	42.0000	-9.3000×10^6
Equation Set				6.1133	42.5215	-9.3970×10^6
Inverse	0.16840×10^8	71.681	12.725			
Error	0.00338×10^8	0.570	0.440	0.1133	0.5215	0.0970×10^6
Patched Conic	0.12836×10^8	123.623	80.842	12.0000	52.0000	-9.3000×10^6
Equation Set				12.1950	51.9827	-9.2914×10^6
Inverse	0.12416×10^8	116.253	86.494			
Error	0.00420×10^8	7.370	5.652	0.1950	0.0173	0.0086×10^6
Patched Conic	0.14110×10^8	99.628	60.516	12.0000	48.0000	-9.3000×10^6
Equation Set				12.1444	47.9186	-9.2868×10^6
Inverse	0.13886×10^8	96.687	62.931			
Error	0.00224×10^8	2.941	2.415	0.1444	0.0814	0.0132×10^6
Patched Conic	0.095594×10^8	76.231	154.850	0	54.0000	-9.3000×10^6
Equation Set				0.1273	54.0877	-9.3076×10^6
Inverse	0.095536×10^8	76.408	155.834			
Error	0.000058×10^8	0.177	0.984	0.1273	0.0877	0.0076×10^6
Patched Conic	0.097213×10^8	53.522	143.231	2.0000	52.0000	-9.3000×10^6
Equation Set				2.1489	52.1134	-9.3094×10^6
Inverse	0.097950×10^8	56.568	141.001			
Error	0.000737×10^8	3.046	2.230	0.1489	0.1134	0.0094×10^6
			AVG	0.1581	0.1422	0.01927×10^6

TABLE C-VIII

TRANSLUNAR TRAJECTORIES USING THE PARABOLIC APPROXIMATION TO ANGULAR MOMENTUM

GENERAL EQUATION SET
MOON AT PERIGEE; 90 HOUR TRIP TIME

	a_1	i_1	i_2	β_{NRT}	λ_{NRT}	GEOCENTRIC ENERGY
Patched Conic	0.26270×10^8	168.446	4.561	0	74.5000	-11.4700×10^6
Equation Set				0.1687	73.8458	-11.4500×10^6
Inverse	0.26123×10^8	171.190	4.252			
Error	0.00147×10^8	2.744	0.309	0.1687	0.6541	0.0200×10^6
Patched Conic	0.23825×10^8	91.765	22.871	0	65.0000	-11.4700×10^6
Equation Set				0.1494	64.5692	-11.4523×10^6
Inverse	0.23616×10^8	91.428	23.620			
Error	0.00209×10^8	0.337	0.749	0.1494	0.4308	0.0177×10^6
Patched Conic	0.23707×10^8	18.169	6.801	0	56.0000	-11.4700×10^6
Equation Set				0.1291	55.6671	-11.4510×10^6
Inverse	0.22743×10^8	17.619	7.199			
Error	0.00964×10^8	0.550	0.398	0.1291	0.3329	0.0190×10^6
Patched Conic	0.23848×10^8	169.359	31.391	7.0000	75.0000	-11.4700×10^6
Equation Set				7.2880	74.5898	-11.4502×10^6
Inverse	0.22743×10^8	172.645	38.155			
Error	0.01105×10^8	3.286	6.764	0.2880	0.4102	0.0198×10^6
Patched Conic	0.25000×10^8	99.910	10.398	7.0000	66.0000	-11.4700×10^6
Equation Set				7.5783	65.4860	-11.4421×10^6
Inverse	0.24677×10^8	99.062	13.242			
Error	0.00328×10^8	0.848	2.844	0.5783	0.5140	0.0279×10^6
Patched Conic	0.22462×10^8	23.316	25.585	7.0000	57.0000	-11.4700×10^6
Equation Set				7.1255	56.7654	-11.4543×10^6
Inverse	0.22243×10^8	22.590	26.700			
Error	0.00219×10^8	0.726	1.115	0.1255	0.2346	0.0157×10^6
Patched Conic	0.17428×10^8	119.455	71.605	14.0000	72.0000	-11.4700×10^6
Equation Set				14.2612	71.8253	-11.4525×10^6
Inverse	No Inverse					
Error				0.2612	0.1747	0.0175×10^6
Patched Conic	0.19028×10^8	96.847	58.614	14.0000	68.0000	-11.4700×10^6
Equation Set				13.9309	67.7128	-11.4592×10^6
Inverse	0.19099×10^8	96.920	57.802			
Error	0.00071×10^8	0.073	0.812	0.0691	0.2872	0.0108×10^6
Patched Conic	0.17658×10^8	67.669	65.996	14.0000	64.5000	-11.4700×10^6
Equation Set				14.0769	64.4401	-11.4642×10^6
Inverse	No Inverse					
Error				0.0769	0.0599	0.0058×10^6
Patched Conic	0.10844×10^8	92.149	160.000	6.7500	72.3870	-11.4700×10^6
Equation Set				6.8267	72.8071	-11.4881×10^6
Inverse	0.10882×10^8	93.163	159.538			
Error	0.00038×10^8	1.014	0.462	0.0767	0.4201	0.0181×10^6
Patched Conic	0.10973×10^8	127.429	160.000	6.0000	75.9670	-11.4700×10^6
Equation Set				5.7679	76.5792	-11.4977×10^6
Inverse	0.10963×10^8	127.712	161.570			
Error	0.00010×10^8	0.283	1.570	0.2321	0.6222	0.0277×10^6
Patched Conic	0.10617×10^8	15.796	160.000	4.0000	66.5520	-11.4700×10^6
Equation Set				3.9026	66.5796	-11.4897×10^6
Inverse	0.10623×10^8	16.930	161.202			
Error	0.00006×10^8	1.134	1.202	0.0974	0.3276	0.0197×10^6
			AVG	0.1877	0.3724	0.0183×10^6

TABLE C–IX

SUMMARY OF ERRORS FOR TRANSLUNAR TRAJECTORIES USING THE PARABOLIC APPROXIMATION TO ANGULAR MOMENTUM

INITIAL CONDITIONS	NO. OF RUNS	EQN. SET*	ERRORS			
				LAT. DEG.	LONG. DEG.	GEO. ENERGY FT^2/SEC^2
H_{PG} = 100 N. MI. H_{PS} = 60 N. MI. $E_E = -8.17 \times 10^6 FT^2/SEC^2$ MOON AT APOGEE	12	H	AVG.	0.1213	0.0900	0.0110×10^6
			MAX.	0.1859	0.1125	0.0148×10^6
H_{PG} = 100 N. MI. H_{PS} = 60 N. MI. $E_E = -9.30 \times 10^6 FT^2/SEC^2$ MOON AT MID-DISTANCE	9	H	AVG.	0.1385	0.1023	0.0121×10^6
			MAX.	0.2199	0.1716	0.0191×10^6
H_{PG} = 100 N. MI. H_{PS} = 60 N. MI. $E_E = -2.8 \times 10^6 FT^2/SEC^2$ MOON AT APOGEE	8	H	AVG.	0.0398	0.0279	0.0064×10^6
			MAX.	0.0558	0.0357	0.0083×10^6
H_{PG} = 10,000 N. MI. H_{PS} = 60 N. MI. $E_E = -8.17 \times 10^6 FT^2/SEC^2$ MOON AT APOGEE	6	H	AVG.	0.2424	0.2684	0.0258×10^6
			MAX.	0.4081	0.4894	0.0520×10^6
H_{PG} = 100 N. MI. H_{PS} = 10,000 N. MI. $E_E = -8.17 \times 10^6 FT^2/SEC^2$ MOON AT APOGEE	10	H	AVG.	0.5691	0.5682	0.0700×10^6
			MAX.	0.9825	1.3443	0.1892×10^6
H_{PG} = 10,000 N. MI. H_{PS} = 10,000 N. MI. $E_E = -8.17 \times 10^6 FT^2/SEC^2$ MOON AT APOGEE	10	H	AVG.	0.5216	0.5109	0.0484×10^6
			MAX.	1.0660	1.1382	0.1320×10^6
H_{PG} = 100 N. MI. H_{PS} = 60 N. MI. $E_E = -9.30 \times 10^6 FT^2/SEC^2$ MOON AT MID-DISTANCE	9	G	AVG.	0.1581	0.1422	0.0193×10^6
			MAX.	0.3429	0.5417	0.0970×10^6
H_{PG} = 100 N. MI. H_{PS} = 60 N. MI. $E_E = -11.47 \times 10^6 FT^2/SEC^2$ MOON AT PERIGEE	12	G	AVG.	0.1877	0.3724	0.0183×10^6
			MAX.	0.5783	0.6541	0.0279×10^6

*H REFERS TO THE HIGH ENERGY EQUATION SET
G REFERS TO THE GENERAL EQUATION SET

H_{PG} = PERIGEE HEIGHT

H_{PS} = PERISELENE HEIGHT

E_E = GEOCENTRIC ENERGY